Chapter 8

Nanotechnology

8.1 Introduction to Nanoparticle Synthesis[1]

The fabrication of nanomaterials with strict control over size, shape, and crystalline structure has inspired the application of nanochemistry to numerous fields including catalysis, medicine, and electronics. The use of nanomaterials in such applications also requires the development of methods for nanoparticle assembly or dispersion in various media. A majority of studies have been aimed at dispersion in aqueous media aimed at their use in medical applications and studies of environmental effects, however, the principles of nanoparticle fabrication and functionalization of nanoparticles transcends their eventual application. Herein, we review the most general routes to nanoparticles of the key types that may have particular application within the oil and gas industry for sensor, composite, or device applications.

Synthesis methods for nanoparticles are typically grouped into two categories: "top-down" and "bottom-up". The first involves division of a massive solid into smaller portions. This approach may involve milling or attrition, chemical methods, and volatilization of a solid followed by condensation of the volatilized components. The second, "bottom-up", method of nanoparticle fabrication involves condensation of atoms or molecular entities in a gas phase or in solution. The latter approach is far more popular in the synthesis of nanoparticles.

Dispersions of nanoparticles are intrinsically thermodynamically metastable, primarily due to their very high surface area, which represents a positive contribution to the free enthalpy of the system. If the activation energies are not sufficiently high, evolution of the nanoparticle dispersion occurs causing an increase in nanoparticle size as typified by an Ostwald ripening process. Thus, highly dispersed nanoparticles are only kinetically stabilized and cannot be prepared under conditions that exceed some threshold, meaning that so-called "soft-chemical" or "*chemie duce*" methods are preferred. In addition, the use of surface stabilization is employed in many nanomaterials to hinder sintering, recrystallization and aggregation.

8.1.1 Bibliography

- J. Gopalakrishnan, *Chem. Mater.*, 1995, **7**, 1265.

8.2 Semiconductor Nanomaterials

8.2.1 Synthesis of Semiconductor Nanoparticles[2]

The most studied non-oxide semiconductors are cadmium chalcogenides (CdE, with E = sulfide, selenide and telluride). CdE nanocrystals were probably the first material used to demonstrate quantum size effects

---

corresponding to a change in the electronic structure with size, i.e., the increase of the band gap energy with the decrease in size of particles (Figure 8.1). These semiconductors nanocrystals are commonly synthesized by thermal decomposition of an organometallic precursor dissolved in an anhydrous solvent containing the source of chalcogenide and a stabilizing material (polymer or capping ligand). Stabilizing molecules bound to the surface of particles control their growth and prevent particle aggregation.


Figure 8.1: Picture of cadmium selenide (CdSe) quantum dots, dissolved in toluene, fluorescing brightly, as they are exposed to an ultraviolet lamp, in three noticeable different colors (blue ∼481 nm, green ∼520 nm, and orange ∼612 nm) due to the quantum dots' bandgap (and thus the wavelength of emitted light) depends strongly on the particle size; the smaller the dot, the shorter the emitted wavelength of light. The "blue" quantum dots have the smallest particle size, the "green" dots are slightly larger, and the "orange" dots are the largest.

Although cadmium chalcogenides are the most studies semiconducting nanoparticles, the methodology for the formation of semiconducting nanoparticles was first demonstrated independently for InP and GaAs, e.g., (8.1). This method has been adapted for a range of semiconductor nanoparticles.

$$InCl_3 + P(SiMe_3)_3 \rightarrow InP + 3 Me_3SiCl$$

(8.1)

In the case of CdE, dimethylcadmium $Cd(CH_3)_2$ is used as a cadmium source and bis(trimethylsilyl)sulfide, $(Me_3Si)_2S$, trioctylphosphine selenide or telluride (TOPSe, TOPTe) serve as sources of selenide in trioctylphosphine oxide (TOPO) used as solvent and capping molecule. The mixture is heated at 230-260 °C over a few hours while modulating the temperature in response to changes in the size distribution as estimated from the absorption spectra of aliquots removed at regular intervals. These particles, capped with TOP/TOPO molecules, are non-aggregated (Figure 8.2) and easily dispersible in organic solvents forming optically clear dispersions. When similar syntheses are performed in the presence of surfactant, strongly anisotropic nanoparticles are obtained, e.g., rod-shaped CdSe nanoparticles can be obtained.
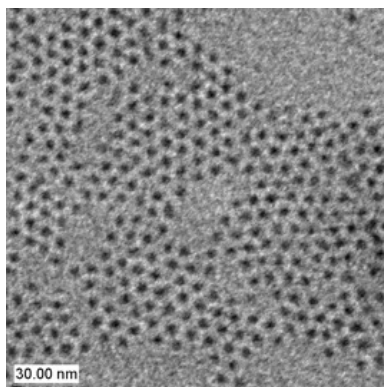
Figure 8.2: TEM image of CdSe nanoparticles.

Because $Cd(CH_3)_2$ is extremely toxic, pyrophoric and explosive at elevated temperature, other Cd sources have been used. CdO appears to be an interesting precursor. CdO powder dissolves in TOPO and HPA or TDPA (tetradecylphosphonic acid) at about 300 °C giving a colorless homogeneous solution. By introducing selenium or tellurium dissolved in TOP, nanocrystals grow to the desired size.

Nanorods of CdSe or CdTe can also be produced by using a greater initial concentration of cadmium as compared to reactions for nanoparticles. This approach has been successfully applied for synthesis of numerous other metal chalcogenides including ZnS, ZnSe, and $Zn_{1-x}Cd_xS$. Similar procedures enable the formation of MnS, PdS, NiS, Cu_2S nanoparticles, nano rods, and nano disks.

8.2.1.1 Bibliography

- C. R. Berry, *Phys. Rev.*, 1967, **161**, 848.
- M. D. Healy, P. E. Laibinis, P. D. Stupik, and A. R. Barron, *J. Chem. Soc., Chem. Commun.*, 1989, 359.
- L. Manna, E. C. Scher, and A. P. Alivisatos, *J. Am. Chem. Soc.*, 2000, **122**, 12700.
- C. B. Murray, D. J. Norris, and M. G. Bawendi, *J. Am. Chem. Soc.*, 1993, **115**, 8706.
- Z. A. Peng and X. Peng, *J. Am. Chem. Soc.*, 2002, **12**, 3343.
- R. L. Wells, C. G. Pitt, A. T. McPhail, A. P. Purdy, S. R. B. Shafieezad, and Hallock *Chem. Mater.*, 1989, **1**, 4.
- X. Zong, Y. Feng, W. Knoll, and H. Man, *J. Am. Chem. Soc.*, 2003, **125**, 13559.

8.2.2 Optical Properties of Group 12-16 (II-VI) Semiconductor Nanoparticles[3]

8.2.2.1 What are Group 12-16 semiconductors?

Semiconductor materials are generally classified on the basis of the periodic table group that their constituent elements belong to. Thus, Group 12-16 semiconductors, formerly called II-VI semiconductors, are materials whose cations are from the Group 12 and anions are from Group 16 in the periodic table (Figure 8.3). Some examples of Group 12-16 semiconductor materials are cadmium selenide (CdSe), zinc sulfide (ZnS), cadmium telluride (CdTe), zinc oxide (ZnO), and mercuric selenide (HgSe) among others.

---

[3]This content is available online at <http://cnx.org/content/m34553/1.1/>.

NOTE: The new IUPAC (International Union of Pure and Applied Chemistry) convention is being followed in this document, to avoid any confusion with regard to conventions used earlier. In the old IUPAC convention, Group 12 was known as Group IIB with the roman numeral 'II' referring to the number of electrons in the outer electronic shells and B referring to being on the right part of the table. However, in the CAS (Chemical Abstracts Service), the alphabet B refers to transition elements as compared to main group elements, though the roman numeral has the same meaning. Similarly, Group 16 was earlier known as Group VI because all the elements in this group have 6 valence shell electrons.

Figure 8.3: The red box indicates the Group 12 and Group 16 elements in the periodic table.

8.2.2.2 What are Group 12-16 (II-VI) semiconductor nanoparticles?

From the Greek word *nanos* - meaning "dwarf" this prefix is used in the metric system to mean 10^{-9} or one billionth (1/1,000,000,000). Thus a nanometer is 10^{-9} or one billionth of a meter, and a nanojoule is 10^{-9} or one billionth of a Joule, etc. A nanoparticle is ordinarily defined as any particle with at least one of its dimensions in the 1 - 100 nm range.

Nanoscale materials often show behavior which is intermediate between that of a bulk solid and that of an individual molecule or atom. An inorganic nanocrystal can be imagined to be comprised of a few atoms or molecules. It thus will behave differently from a single atom; however, it is still smaller than a macroscopic solid, and hence will show different properties. For example, if one would compare the chemical reactivity of a bulk solid and a nanoparticle, the latter would have a higher reactivity due to a significant fraction of the total number of atoms being on the surface of the particle. Properties such as boiling point, melting point, optical properties, chemical stability, electronic properties, etc. are all different in a nanoparticle as compared to its bulk counterpart. In the case of Group 12-16 semiconductors, this reduction in size from bulk to the nanoscale results in many size dependent properties such as varying band gap energy, optical and electronic properties.

8.2.2.3 Optical properties of semiconductor quantum nanoparticles

In the case of semiconductor nanocrystals, the effect of the size on the optical properties of the particles is very interesting. Consider a Group 12-16 semiconductor, cadmium selenide (CdSe). A 2 nm sized CdSe

crystal has a blue color fluorescence whereas a larger nanocrystal of CdSe of about 6 nm has a dark red fluorescence (Figure 8.4). In order to understand the size dependent optical properties of semiconductor nanoparticles, it is important to know the physics behind what is happening at the nano level.


Figure 8.4: Fluorescing CdSe quantum dots synthesized in a heat transfer liquid of different sizes (M. S. Wong, Rice University).

8.2.2.3.1 Energy levels in a semiconductor

The electronic structure of any material is given by a solution of Schrödinger equations with boundary conditions, depending on the physical situation. The electronic structure of a semiconductor (Figure 8.5) can be described by the following terms:
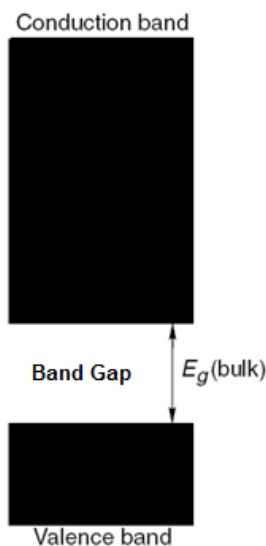
Figure 8.5: Simplified representation of the energy levels in a bulk semiconductor.

8.2.2.3.1.1 Energy level

By the solution of Schrödinger's equations, the electrons in a semiconductor can have only certain allowable energies, which are associated with energy levels. No electrons can exist in between these levels, or in other words can have energies in between the allowed energies. In addition, from Pauli's Exclusion Principle, only 2 electrons with opposite spin can exist at any one energy level. Thus, the electrons start filling from the lowest energy levels. Greater the number of atoms in a crystal, the difference in allowable energies become very small, thus the distance between energy levels decreases. However, this distance can never be zero. For a bulk semiconductor, due to the large number of atoms, the distance between energy levels is very small and for all practical purpose the energy levels can be described as continuous (Figure 8.5).

8.2.2.3.1.2 Band gap

From the solution of Schrödinger's equations, there are a set of energies which is not allowable, and thus no energy levels can exist in this region. This region is called the band gap and is a quantum mechanical phenomenon (Figure 8.5). In a bulk semiconductor the bandgap is fixed; whereas in a quantum dot nanoparticle the bandgap varies with the size of the nanoparticle.

8.2.2.3.1.3 Valence band

In bulk semiconductors, since the energy levels can be considered as continuous, they are also termed as energy bands. Valence band contains electrons from the lowest energy level to the energy level at the lower edge of the bandgap (Figure 8.5). Since filling of energy is from the lowest energy level, this band is usually almost full.

8.2.2.3.1.4 Conduction band

The conduction band consists of energy levels from the upper edge of the bandgap and higher (Figure 8.5). To reach the conduction band, the electrons in the valence band should have enough energy to cross the band gap. Once the electrons are excited, they subsequently relax back to the valence band (either radiatively or non-radiatively) followed by a subsequent emission of radiation. This property is responsible for most of the applications of quantum dots.

8.2.2.3.1.5 Exciton and exciton Bohr radius

When an electron is excited from the valence band to the conduction band, corresponding to the electron in the conduction band a hole (absence of electron) is formed in the valence band. This electron pair is called an exciton. Excitons have a natural separation distance between the electron and hole, which is characteristic of the material. This average distance is called exciton Bohr radius. In a bulk semiconductor, the size of the crystal is much larger than the exciton Bohr radius and hence the exciton is free to move throughout the crystal.

8.2.2.3.2 Energy levels in a quantum dot semiconductor

Before understanding the electronic structure of a quantum dot semiconductor, it is important to understand what a quantum dot nanoparticle is. We earlier studied that a nanoparticle is any particle with one of its dimensions in the 1 - 100 nm. A quantum dot is a nanoparticle with its diameter on the order of the materials exciton Bohr radius. Quantum dots are typically 2 - 10 nm wide and approximately consist of 10 to 50 atoms. With this understanding of a quantum dot semiconductor, the electronic structure of a quantum dot semiconductor can be described by the following terms.
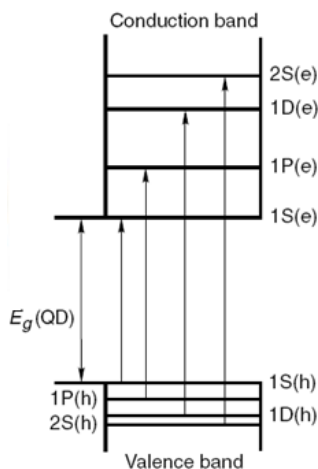
Figure 8.6: Energy levels in quantum dot. Allowed optical transitions are shown. Adapted from T. Pradeep, *Nano: The Essentials. Understanding Nanoscience and Nanotechnology*, Tata McGraw-Hill, New Delhi (2007).

8.2.2.3.2.1 Quantum confinement

When the size of the semiconductor crystal becomes comparable or smaller than the exciton Bohr radius, the quantum dots are in a state of quantum confinement. As a result of quantum confinement, the energy levels in a quantum dot are discrete (Figure 8.6) as opposed to being continuous in a bulk crystal (Figure 8.5).

8.2.2.3.2.2 Discrete energy levels

In materials that have small number of atoms and are considered as quantum confined, the energy levels are separated by an appreciable amount of energy such that they are not continuous, but are discrete (see Figure 8.6). The energy associated with an electron (equivalent to conduction band energy level) is given by is given by (8.2), where h is the Planck's constant, m_e is the effective mass of electron and n is the quantum number for the conduction band states, and n can take the values 1, 2, 3 and so on. Similarly, the energy associated with the hole (equivalent to valence band energy level) is given by (8.3), where n' is the quantum number for the valence states, and n' can take the values 1, 2, 3, and so on. The energy increases as one goes higher in the quantum number. Since the electron mass is much smaller than that of the hole, the electron levels are separated more widely than the hole levels.

$$E^e = \frac{h^2 n^2}{8\pi^2 m_e d^2}$$

$$\tag{8.2}$$

$$E^h = \frac{h^2 n'^2}{8\pi^2 m_h d^2}$$

$$\tag{8.3}$$

8.2.2.3.2.3 Tunable band gap

As seen from (8.2) and (8.3), the energy levels are affected by the diameter of the semiconductor particles. If the diameter is very small, since the energy is dependent on inverse of diameter squared, the energy levels of the upper edge of the band gap (lowest conduction band level) and lower edge of the band gap (highest valence band level) change significantly with the diameter of the particle and the effective mass of the electron and the hole, resulting in a size dependent tunable band gap. This also results in the discretization of the energy levels.

Qualitatively, this can be understood in the following way. In a bulk semiconductor, the addition or removal of an atom is insignificant compared to the size of the bulk semiconductor, which consists of a large number of atoms. The large size of bulk semiconductors makes the changes in band gap so negligible on the addition of an atom, that it is considered as a fixed band gap. In a quantum dot, addition of an atom does make a difference, resulting in the tunability of band gap.

8.2.2.3.3 UV-visible absorbance

Due to the presence of discrete energy levels in a QD, there is a widening of the energy gap between the highest occupied electronic states and the lowest unoccupied states as compared to the bulk material. As a consequence, the optical properties of the semiconductor nanoparticles also become size dependent.

The minimum energy required to create an exciton is the defined by the band gap of the material, i.e., the energy required to excite an electron from the highest level of valence energy states to the lowest level of the conduction energy states. For a quantum dot, the bandgap varies with the size of the particle. From (8.2) and (8.3), it can be inferred that the band gap becomes higher as the particle becomes smaller. This means that for a smaller particle, the energy required for an electron to get excited is higher. The relation between energy and wavelength is given by (8.4), where h is the Planck's constant, c is the speed of light, λ

is the wavelength of light. Therefore, from (8.4) to cross a bandgap of greater energy, shorter wavelengths of light are absorbed, i.e., a blue shift is seen.

$$E = \frac{hc}{\lambda}$$

(8.4)

For Group 12-16 semiconductors, the bandgap energy falls in the UV-visible range. That is ultraviolet light or visible light can be used to excite an electron from the ground valence states to the excited conduction states. In a bulk semiconductor the band gap is fixed, and the energy states are continuous. This results in a rather uniform absorption spectrum (Figure 8.7a).
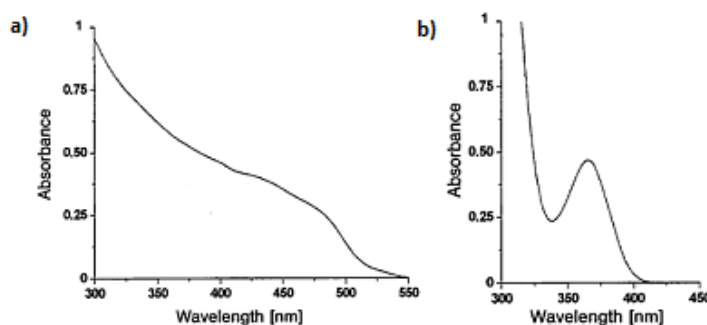
Figure 8.7: UV-vis spectra of (a) bulk CdS and (b) 4 nm CdS. Adapted from G. Kickelbick, *Hybrid Materials: Synthesis, Characterization and Applications*, Wiley-VCH, Weinheim (2007).

In the case of Group 12-16 quantum dots, since the bandgap can be changed with the size, these materials can absorb over a range of wavelengths. The peaks seen in the absorption spectrum (Figure 8.7b) correspond to the optical transitions between the electron and hole levels. The minimum energy and thus the maximum wavelength peak corresponds to the first exciton peak or the energy for an electron to get excited from the highest valence state to the lowest conduction state. The quantum dot will not absorb wavelengths of energy longer than this wavelength. This is known as the absorption onset.

8.2.2.3.4 Fluorescence

Fluorescence is the emission of electromagnetic radiation in the form of light by a material that has absorbed a photon. When a semiconductor quantum dot (QD) absorbs a photon/energy equal to or greater than its band gap, the electrons in the QD's get excited to the conduction state. This excited state is however not stable. The electron can relax back to its ground state by either emitting a photon or lose energy via heat losses. These processes can be divided into two categories – radiative decay and non-radiative decay. Radiative decay is the loss of energy through the emission of a photon or radiation. Non-radiative decay involves the loss of heat through lattice vibrations and this usually occurs when the energy difference between the levels is small. Non-radiative decay occurs much faster than radiative decay.

Usually the electron relaxes to the ground state through a combination of both radiative and non-radiative decays. The electron moves quickly through the conduction energy levels through small non-radiative decays and the final transition across the band gap is via a radiative decay. Large nonradiative decays don't occur across the band gap because the crystal structure can't withstand large vibrations without breaking the bonds of the crystal. Since some of the energy is lost through the non-radiative decay, the energy of the emitted photon, through the radiative decay, is much lesser than the absorbed energy. As a result the

wavelength of the emitted photon or fluorescence is longer than the wavelength of absorbed light. This energy difference is called the Stokes shift. Due this Stokes shift, the emission peak corresponding to the absorption band edge peak is shifted towards a higher wavelength (lower energy), i.e., Figure 8.8.
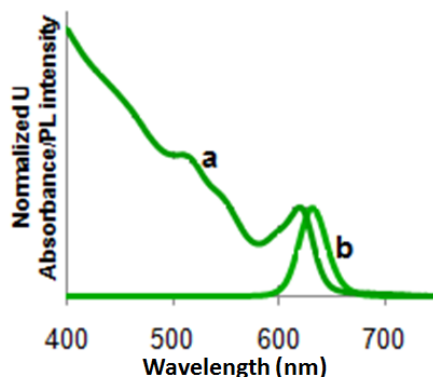
Figure 8.8: Absorption spectra (a) and emission spectra (b) of CdSe tetrapod.

Intensity of emission versus wavelength is a bell-shaped Gaussian curve. As long as the excitation wavelength is shorter than the absorption onset, the maximum emission wavelength is independent of the excitation wavelength. Figure 8.8 shows a combined absorption and emission spectrum for a typical CdSe tetrapod.

8.2.2.3.5 Factors affecting the optical properties of NPs

There are various factors that affect the absorption and emission spectra for Group 12-16 semiconductor quantum crystals. Fluorescence is much more sensitive to the background, environment, presence of traps and the surface of the QDs than UV-visible absorption. Some of the major factors influencing the optical properties of quantum nanoparticles include:

- **Surface defects, imperfection of lattice, surface charges** – The surface defects and imperfections in the lattice structure of semiconductor quantum dots occur in the form of unsatisfied valencies. Similar to surface charges, unsatisfied valencies provide a sink for the charge carriers, resulting in unwanted recombinations.
- **Surface ligands** – The presence of surface ligands is another factor that affects the optical properties. If the surface ligand coverage is a 100%, there is a smaller chance of surface recombinations to occur.
- **Solvent polarity** – The polarity of solvents is very important for the optical properties of the nanoparticles. If the quantum dots are prepared in organic solvent and have an organic surface ligand, the more non-polar the solvent, the particles are more dispersed. This reduces the loss of electrons through recombinations again, since when particles come in close proximity to each other, increases the non-radiative decay events.

8.2.2.3.6 Applications of the optical properties of Group 12-16 semiconductor NPs

The size dependent optical properties of NP's have many applications from biomedical applications to solar cell technology, from photocatalysis to chemical sensing. Most of these applications use the following unique properties.

For applications in the field of nanoelectronics, the sizes of the quantum dots can be tuned to be comparable to the scattering lengths, reducing the scattering rate and hence, the signal to noise ratio. For Group 12-16 QDs to be used in the field of solar cells, the bandgap of the particles can be tuned so as to form absorb energy over a large range of the solar spectrum, resulting in more number of excitons and hence more electricity. Since the nanoparticles are so small, most of the atoms are on the surface. Thus, the surface to volume ratio is very large for the quantum dots. In addition to a high surface to volume ratio, the Group 12-16 QDs respond to light energy. Thus quantum dots have very good photocatalytic properties. Quantum dots show fluorescence properties, and emit visible light when excited. This property can be used for applications as biomarkers. These quantum dots can be tagged to drugs to monitor the path of the drugs. Specially shaped Group 12-16 nanoparticles such as hollow shells can be used as drug delivery agents. Another use for the fluorescence properties of Group 12-16 semiconductor QDs is in color-changing paints, which can change colors according to the light source used.

8.2.2.3.7 Bibliography

- M. J. Schulz, V. N. Shanov, and Y. Yun, *Nanomedicine - Design of Particles, Sensors, Motors, Implants, Robots, and Devices*, Artech House, London (2009).
- S. V. Gapoenko, *Optical Properties of Semiconductor Nanocrystals*, Cambridge University Press, Cambridge (2003).
- T. Pradeep, *Nano: The Essentials. Understanding Nanoscience and Nanotechnology*, Tata McGraw-Hill, New Delhi (2007).
- G. Schmid, *Nanoparticles: From Theory to Application*, Wiley-VCH, Weinheim (2004).
- A. L. Rogach, *Semiconductor Nanocrystal Quantum Dots. Synthesis, Assembly, Spectroscopy and Applications*, Springer Wien, New York (2008).
- G. Kickelbick, *Hybrid Materials: Synthesis, Characterization and Applications*, Wiley-VCH, Weinheim (2007).

8.2.3 Characterization of Group 12-16 (II-VI) Semiconductor Nanoparticles by UV-visible Spectroscopy[4]

Quantum dots (QDs) as a general term refer to nanocrystals of semiconductor materials, in which the size of the particles are comparable to the natural characteristic separation of an electron-hole pair, otherwise known as the exciton Bohr radius of the material. When the size of the semiconductor nanocrystal becomes this small, the electronic structure of the crystal is governed by the laws of quantum physics. Very small Group 12-16 (II-VI) semiconductor nanoparticle quantum dots, in the order of 2 - 10 nm, exhibit significantly different optical and electronic properties from their bulk counterparts. The characterization of size dependent optical properties of Group 12-16 semiconductor particles provide a lot of qualitative and quantitative information about them – size, quantum yield, monodispersity, shape and presence of surface defects. A combination of information from both the UV-visible absorption and fluorescence, complete the analysis of the optical properties.

8.2.3.1 UV-visible absorbance spectroscopy

Absorption spectroscopy, in general, refers to characterization techniques that measure the absorption of radiation by a material, as a function of the wavelength. Depending on the source of light used, absorption spectroscopy can be broadly divided into infrared and UV-visible spectroscopy. The band gap of Group 12-16 semiconductors is in the UV-visible region. This means the minimum energy required to excite an electron from the valence states of the Group 12-16 semiconductor QDs to its conduction states, lies in the UV-visible region. This is also a reason why most of the Group 12-16 semiconductor quantum dot solutions are colored.

---

[4]This content is available online at <http://cnx.org/content/m34601/1.1/>.

This technique is complementary to fluorescence spectroscopy, in that UV-visible spectroscopy measures electronic transitions from the ground state to the excited state, whereas fluorescence deals with the transitions from the excited state to the ground state. In order to characterize the optical properties of a quantum dot, it is important to characterize the sample with both these techniques

In quantum dots, due to the very small number of atoms, the addition or removal of one atom to the molecule changes the electronic structure of the quantum dot dramatically. Taking advantage of this property in Group 12-16 semiconductor quantum dots, it is possible to change the band gap of the material by just changing the size of the quantum dot. A quantum dot can absorb energy in the form of light over a range of wavelengths, to excite an electron from the ground state to its excited state. The minimum energy that is required to excite an electron, is dependent on the band gap of the quantum dot. Thus, by making accurate measurements of light absorption at different wavelengths in the ultraviolet and visible spectrum, a correlation can be made between the band gap and size of the quantum dot. Group 12-16 semiconductor quantum dots are of particular interest, since their band gap lies in the visible region of the solar spectrum.

The UV-visible absorbance spectroscopy is a characterization technique in which the absorbance of the material is studied as a function of wavelength. The visible region of the spectrum is in the wavelength range of 380 nm (violet) to 740 nm (red) and the near ultraviolet region extends to wavelengths of about 200 nm. The UV-visible spectrophotometer analyzes over the wavelength range $200 - 900$ nm.

When the Group 12-16 semiconductor nanocrystals are exposed to light having an energy that matches a possible electronic transition as dictated by laws of quantum physics, the light is absorbed and an exciton pair is formed. The UV-visible spectrophotometer records the wavelength at which the absorption occurs along with the intensity of the absorption at each wavelength. This is recorded in a graph of absorbance of the nanocrystal versus wavelength.

8.2.3.2 Instrumentation

A working schematic of the UV-visible spectrophotometer is shown in Figure 8.9.
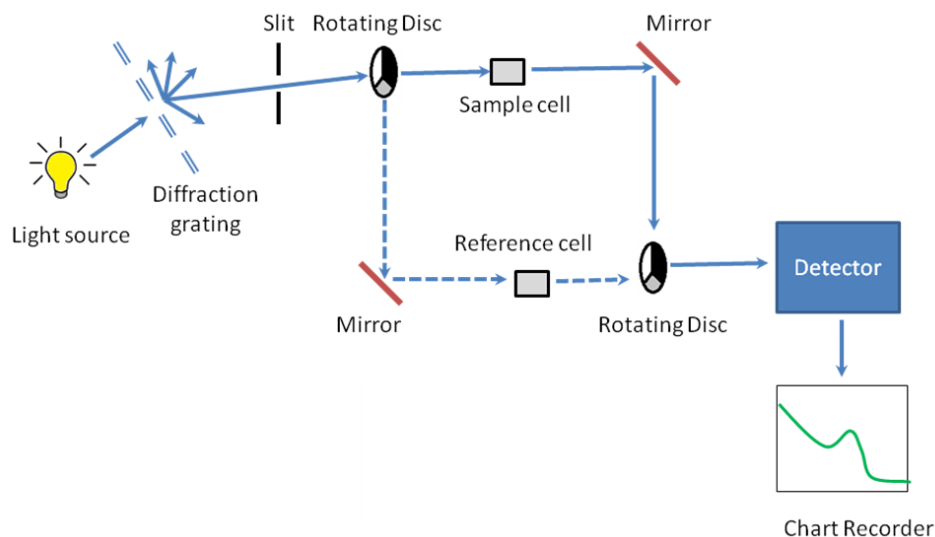
Figure 8.9: Schematic of UV-visible spectrophotometer.

8.2.3.2.1 The light source

Since it is a UV-vis spectrophotometer, the light source (Figure 8.9) needs to cover the entire visible and the near ultra-violet region (200 - 900 nm). Since it is not possible to get this range of wavelengths from a single lamp, a combination of a deuterium lamp for the UV region of the spectrum and tungsten or halogen lamp for the visible region is used. This output is then sent through a diffraction grating as shown in the schematic.

8.2.3.2.2 The diffraction grating and the slit

The beam of light from the visible and/or UV light source is then separated into its component wavelengths (like a very efficient prism) by a diffraction grating (Figure 8.9). Following the slit is a slit that sends a monochromatic beam into the next section of the spectrophotometer.

8.2.3.2.3 Rotating discs

Light from the slit then falls onto a rotating disc (Figure 8.9). Each disc consists of different segments – an opaque black section, a transparent section and a mirrored section. If the light hits the transparent section, it will go straight through the sample cell, get reflected by a mirror, hits the mirrored section of a second rotating disc, and then collected by the detector. Else if the light hits the mirrored section, gets reflected by a mirror, passes through the reference cell, hits the transparent section of a second rotating disc and then collected by the detector. Finally if the light hits the black opaque section, it is blocked and no light passes through the instrument, thus enabling the system to make corrections for any current generated by the detector in the absence of light.

8.2.3.2.4 Sample cell, reference cell and sample preparation

For liquid samples, a square cross section tube sealed at one end is used. The choice of cuvette depends on the following factors:

- **Type of solvent** - For aqueous samples, specially designed rectangular quartz, glass or plastic cuvettes are used. For organic samples glass and quartz cuvettes are used.
- **Excitation wavelength** – Depending on the size and thus, bandgap of the 12-16 semiconductor nanoparticles, different excitation wavelengths of light are used. Depending on the excitation wavelength, different materials are used

Cuvette	Wavelength (nm)
Visible only glass	380 - 780
Visible only plastic	380 - 780
UV plastic	220 - 780
Quartz	200 - 900

Table 8.1: Cuvette materials and their wavelengths.

- **Cost** – Plastic cuvettes are the least expensive and can be discarded after use. Though quartz cuvettes have the maximum utility, they are the most expensive, and need to reused. Generally, disposable plastic cuvettes are used when speed is more important than high accuracy.

The best cuvettes need to be very clear and have no impurities that might affect the spectroscopic reading. Defects on the cuvette such as scratches, can scatter light and hence should be avoided. Some cuvettes are clear only on two sides, and can be used in the UV-Visible spectrophotometer, but cannot be used for

fluorescence spectroscopy measurements. For Group 12-16 semiconductor nanoparticles prepared in organic solvents, the quartz cuvette is chosen.

In the sample cell the quantum dots are dispersed in a solvent, whereas in the reference cell the pure solvent is taken. It is important that the sample be very dilute (maximum first exciton absorbance should not exceed 1 au) and the solvent is not UV-visible active. For these measurements, it is required that the solvent does not have characteristic absorption or emission in the region of interest. Solution phase experiments are preferred, though it is possible to measure the spectra in the solid state also using thin films, powders, etc. The instrumentation for solid state UV-visible absorption spectroscopy is slightly different from the solution phase experiments and is beyond the scope of discussion.

8.2.3.2.5 Detector

Detector converts the light into a current signal that is read by a computer. Higher the current signal, greater is the intensity of the light. The computer then calculates the absorbance using the in (8.5), where A denotes absorbance, I is sample cell intensity and I_o is the reference cell intensity.

$$A = \log_{10}(I_0/I)$$

(8.5)

The following cases are possible:

- Where $I < I_0$ and $A < 0$. This usually occurs when the solvent absorbs in the wavelength range. Preferably the solvent should be changed, to get an accurate reading for actual reference cell intensity.
- Where $I = I_0$ and $A = 0$. This occurs when pure solvent is put in both reference and sample cells. This test should always be done before testing the sample, to check for the cleanliness of the cuvettes.
- When $A = 1$. This occurs when 90% or the light at a particular wavelength has been absorbed, which means that only 10% is seen at the detector. So I_0/I becomes $100/10 = 10$. $\log_{10}$ of 10 is 1.
- When $A > 1$. This occurs in extreme case where more than 90% of the light is absorbed.

8.2.3.2.6 Output

The output is the form of a plot of absorbance against wavelength, e.g., Figure 8.10.
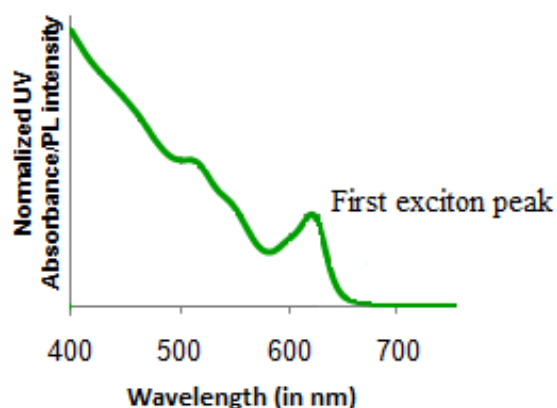
Figure 8.10: Representative UV-visble absorption spectrum for CdSe tetrapods.

8.2.3.3 Beer-Lambert law

In order to make comparisons between different samples, it is important that all the factors affecting absorbance should be constant except the sample itself.

8.2.3.3.1 Effect of concentration on absorbance

The extent of absorption depends on the number of absorbing nanoparticles or in other words the concentration of the sample. If it is a reasonably concentrated solution, it will have a high absorbance since there are lots of nanoparticles to interact with the light. Similarly in an extremely dilute solution, the absorbance is very low. In order to compare two solutions, it is important that we should make some allowance for the concentration.

8.2.3.3.2 Effect of container shape

Even if we had the same concentration of solutions, if we compare two solutions – one in a rectagular shaped container (e.g., Figure 8.11) so that light travelled 1 cm through it and the other in which the light travelled 100 cm through it, the absorbance would be different. This is because if the length the light travelled is greater, it means that the light interacted with more number of nanocrystals, and thus has a higher absorbance. Again, in order to compare two solutions, it is important that we should make some allowance for the concentration.

Figure 8.11: A typical rectangular cuvette for UV-visible spectroscopy.

8.2.3.3.3 The law

The Beer-Lambert law addresses the effect of concentration and container shape as shown in (8.5), (8.6) and (8.7), where A denotes absorbance; ε is the molar absorptivity or molar absorption coefficient; l is the path length of light (in cm); and c is the concentration of the solution (mol/dm^3).

$$\log_{10}(I_0/I) = \varepsilon l c$$

$$(8.6)$$

$$A = \varepsilon l c$$

$$(8.7)$$

8.2.3.3.4 Molar absorptivity

From the Beer-Lambert law, the molar absorptivity 'ε' can be expressed as shown in (8.8).

$$c = A/l\varepsilon$$

(8.8)

Molar absorptivity corrects for the variation in concentration and length of the solution that the light passes through. It is the value of absorbance when light passes through 1 cm of a 1 mol/dm^3 solution.

8.2.3.3.5 Limitations of Beer-Lambert law

The linearity of the Beer-Lambert law is limited by chemical and instrumental factors.

- At high concentrations (> 0.01 M), the relation between absorptivity coefficient and absorbance is no longer linear. This is due to the electrostatic interactions between the quantum dots in close proximity.
- If the concentration of the solution is high, another effect that is seen is the scattering of light from the large number of quantum dots.
- The spectrophotometer performs calculations assuming that the refractive index of the solvent does not change significantly with the presence of the quantum dots. This assumption only works at low concentrations of the analyte (quantum dots).
- Presence of stray light.

8.2.3.4 Analysis of data

The data obtained from the spectrophotometer is a plot of absorbance as a function of wavelength. Quantitative and qualitative data can be obtained by analysing this information

8.2.3.4.1 Quantitative Information

The band gap of the semiconductor quantum dots can be tuned with the size of the particles. The minimum energy for an electron to get excited from the ground state is the energy to cross the band gap. In an absorption spectra, this is given by the first exciton peak at the maximum wavelength ($\lambda_{\max}$).

8.2.3.4.1.1 Size of the quantum dots

The size of quantum dots can be approximated corresponding to the first exciton peak wavelength. Emperical relationships have been determined relating the diameter of the quantum dot to the wavelength of the first exciton peak. The Group 12-16 semiconductor quantum dots that they studied were cadmium selenide (CdSe), cadmium telluride (CdTe) and cadmium sulfide (CdS). The empirical relationships are determined by fitting experimental data of absorbance versus wavelength of known sizes of particles. The empirical equations determined are given for CdTe, CdSe, and CdS in (8.9), (8.10) and (8.11) respectively, where D is the diameter and λ is the wavelength corresponding to the first exciton peak. For example, if the first exciton peak of a CdSe quantum dot is 500 nm, the corresponding diameter of the quantum dot is 2.345 nm and for a wavelength of 609 nm, the corresponding diameter is 5.008 nm.

$$D = (9.8127 \times 10^{-7})\lambda^3 - (1.7147 \times 10^{-3})\lambda^2 + (1.0064)\lambda - 194.84$$

(8.9)

$$D = (1.6122 \times 10^{-7})\lambda^3 - (2.6575 \times 10^{-6})\lambda^2 + (1.6242 \times 10^{-3})\lambda + 41.57$$

(8.10)

$$D = (-6.6521 \times 10^{-8})\lambda^3 + (1.9577 \times 10^{-4})\lambda^2 - (9.2352 \times 10^{-2})\lambda + 13.29$$

(8.11)

8.2.3.4.1.2 Concentration of sample

Using the Beer-Lambert law, it is possible to calculate the concentration of the sample if the molar absorptivity for the sample is known. The molar absorptivity can be calculated by recording the absorbance of a standard solution of 1 mol/dm^3 concentration in a standard cuvette where the light travels a constant distance of 1 cm. Once the molar absorptivity and the absorbance of the sample are known, with the length the light travels being fixed, it is possible to determine the concentration of the sample solution.

Empirical equations can be determined by fitting experimental data of extinction coefficient per mole of Group 12-16 semiconductor quantum dots, at 250 °C, to the diameter of the quantum dot, (8.12), (8.13), and (8.14).

$$\varepsilon = 10043 \text{ x } D^{2.12}$$
(8.12)

$$\varepsilon = 5857 \text{ x } D^{2.65}$$
(8.13)

$$\varepsilon = 21536 \text{ x } D^{2.3}$$
(8.14)

The concentration of the quantum dots can then be then be determined by using the Beer Lambert law as given by (8.8).

8.2.3.4.2 Qualitative Information

Apart from quantitative data such as the size of the quantum dots and concentration of the quantum dots, a lot of qualitative information can be derived from the absorption spectra.

8.2.3.4.2.1 Size distribution

If there is a very narrow size distribution, the first exciton peak will be very sharp (Figure 8.12). This is because due to the narrow size distribution, the differences in band gap between different sized particles will be very small and hence most of the electrons will get excited over a smaller range of wavelengths. In addition, if there is a narrow size distribution, the higher exciton peaks are also seen clearly.
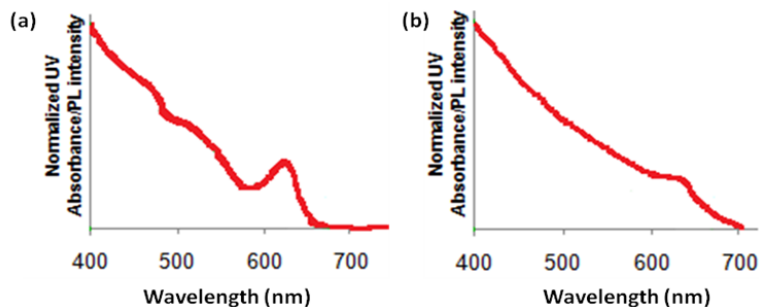
Figure 8.12: Narrow emission spectra (a) and broad emission spectra (b) of CdSe QDs.

8.2.3.4.2.2 Shaped particles

In the case of a spherical quantum dot, in all dimensions, the particle is quantum confined (Figure 8.13). In the case of a nanorod, whose length is not in the quantum regime, the quantum effects are determined by the width of the nanorod. Similar is the case in tetrapods or four legged structures. The quantum effects are determined by the thickness of the arms. During the synthesis of the shaped particles, the thickness of the rod or the arm of the tetrapod does not vary among the different particles, as much as the length of the rods or arms changes. Since the thickness of the rod or tetrapod is responsible for the quantum effects, the absorption spectrum of rods and tetrapods has sharper features as compared to a quantum dot. Hence, qualitatively it is possible to differentiate between quantum dots and other shaped particles.
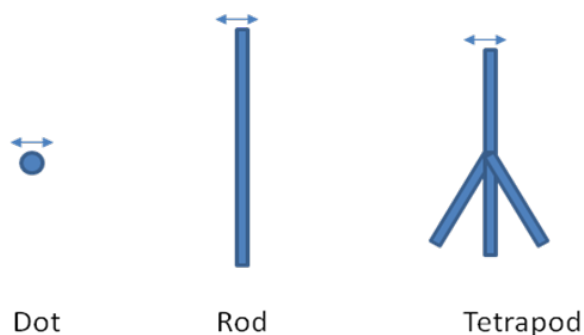
Figure 8.13: Different shaped nanoparticles with the arrows indicating the dimension where quantum confinement effects are observed.

8.2.3.4.2.3 Crystal lattice information

In the case of CdSe semiconductor quantum dots it has been shown that it is possible to estimate the crystal lattice of the quantum dot from the adsorption spectrum (Figure 8.14), and hence determine if the structure is zinc blend or wurtzite.
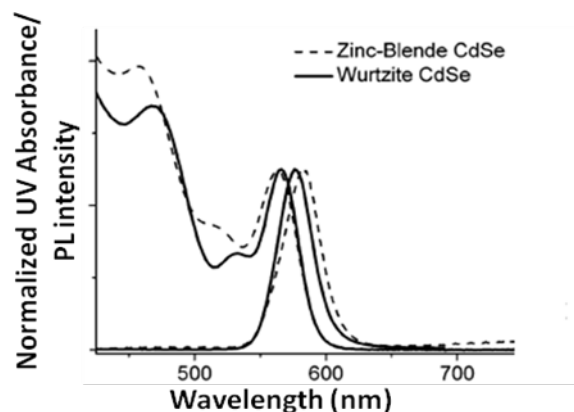
Figure 8.14: Zinc blende and wurtzite CdSe absorption spectra. Adapted from J. Jasieniak, C. Bullen, J. van Embden, and P. Mulvaney, *J. Phys. Chem. B*, 2005, **109**, 20665.

### 8.2.3.5 UV-vis absorption spectra of Group 12-16 semiconductor nanoparticles

8.2.3.5.1 Cadmium selenide

Cadmium selenide (CdSe) is one of the most popular Group 12-16 semiconductors. This is mainly because the band gap (712 nm or 1.74 eV) energy of CdSe. Thus, the nanoparticles of CdSe can be engineered to have a range of band gaps throughout the visible range, corresponding to the major part of the energy that comes from the solar spectrum. This property of CdSe along with its fluorescing properties is used in a variety of applications such as solar cells and light emitting diodes. Though cadmium and selenium are known carcinogens, the harmful biological effects of CdSe can be overcome by coating the CdSe with a layer of zinc sulfide. Thus CdSe, can also be used as bio-markers, drug-delivery agents, paints and other applications.

A typical absorption spectrum of narrow size distribution wurtzite CdSe quantum dot is shown in Figure 8.15. A size evolving absorption spectra is shown in Figure 8.16. However, a complete analysis of the sample is possible only by also studying the fluorescence properties of CdSe.
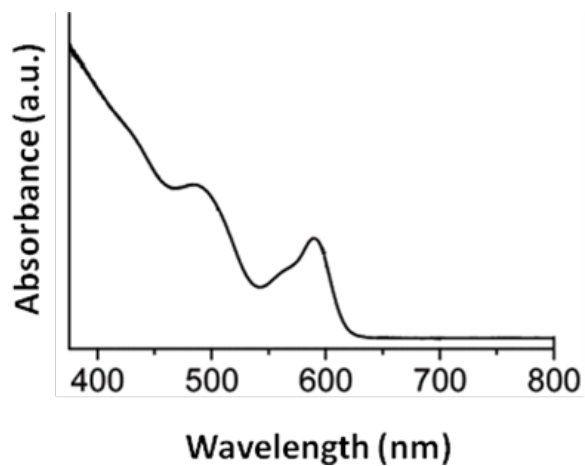
Figure 8.15: Wurtzite CdSe quantum dot. Adapted from X. Zhong, Y. Feng, and Y. Zhang, *J. Phys. Chem. C*, 2007, **111**, 526.
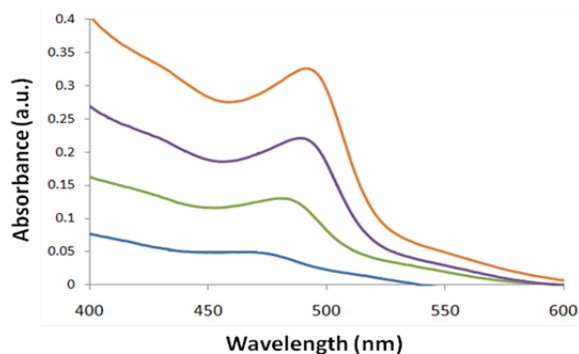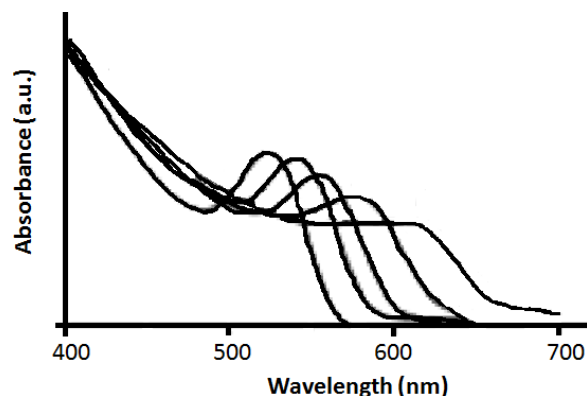

Figure 8.16: Size evolving absorption spectra of CdSe quantum dots.

8.2.3.5.2 Cadmium telluride (CdTe)

Cadmium telluride has a band gap of 1.44 eV (860 nm) and as such it absorbs in the infrared region. Like CdSe, the sizes of CdTe can be engineered to have different band edges and thus, different absorption spectra as a function of wavelength. A typical CdTe spectra is shown in Figure 8.17. Due to the small bandgap energy of CdTe, it can be used in tandem with CdSe to absorb in a greater part of the solar spectrum.

Figure 8.17: Size evolving absorption spectra of CdTe quantum dots from 3 nm to 7 nm. Adapted from C. Qi-Fan, W. Wen-Xing, G. Ying-Xin, L. Meng-Ying, X. Shu-Kun and Z. Xiu-Juan, *Chin. J. Anal. Chem.*, 2007, **35**, 135.

8.2.3.5.3 Other Group 12-16 semiconductor systems

Table 8.2 shows the bulk band gap of other Group 12-16 semiconductor systems. The band gap of ZnS falls in the UV region, while those of ZnSe, CdS, and ZnTe fall in the visible region.

Material	Band gap (eV)	Wavelength (nm)
ZnS	3.61	343.2
ZnSe	2.69	460.5
ZnTe	2.39	518.4
CdS	2.49	497.5
CdSe	1.74	712.1
CdTe	1.44	860.3

Table 8.2: Bulk band gaps of different Group 12-16 semiconductors.

8.2.3.5.4 Heterostructures of Group 12-16 semiconductor systems

It is often desirable to have a combination of two Group 12-16 semiconductor system quantum heterostructures of different shapes like dots and tetrapods, for applications in solar cells, bio-markers, etc. Some of the most interesting systems are ZnS shell-CdSe core systems, such as the CdSe/CdS rods and tetrapods.

Figure 8.18 shows a typical absorption spectra of CdSe-ZnS core-shell system. This system is important because of the drastically improved fluorescence properties because of the addition of a wide band gap ZnS shell than the core CdSe. In addition with a ZnS shell, CdSe becomes bio-compatible.
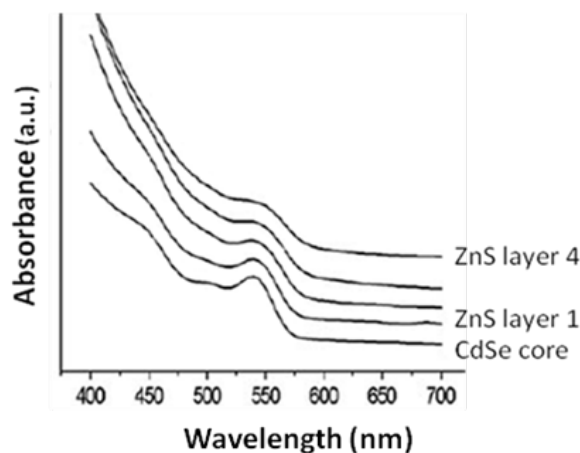
Figure 8.18: Absorption spectra of CdSe core, ZnS shell. Adapted from C. Qing-Zhu, P. Wang, X. Wang and Y. Li, *Nanoscale Res. Lett.*, 2008, **3**, 213.

A CdSe seed, CdS arm nanorods system is also interesting. Combining CdSe and CdS in a single nanostructure creates a material with a mixed dimensionality where holes are confined to CdSe while electrons can move freely between CdSe and CdS phases.

8.2.3.6 Bibliography

- S. V. Gapoenko, *Optical Properties of Semiconductor Nanocrystals*, Cambridge University Press, Cambridge (2003).
- W. W. Yu, L. Qu, W. Guo, and X. Peng, *Chem. Mater.*, 2003, **15**, 2854.
- J. Jasieniak, C. Bullen, J. van Embden, and P. Mulvaney, *J. Phys. Chem. B*, 2005, **109**, 20665.
- X. Zhong, Y. Feng, and Y. Zhang, *J. Phys. Chem. C*, 2007, **111**, 526.
- D. V. Talapin, J. H. Nelson, E. V. Shevchenko, S. Aloni, B. Sadtler, and A. P. Alivisatos, *Nano Lett.*, 2007, **7**, 2951.
- C. Qing-Zhu, P. Wang, X. Wang, and Y. Li, *Nanoscale Res. Lett.*, 2008, **3**, 213.
- C. Qi-Fan, W. Wen-Xing, G. Ying-Xin, L. Meng-Ying, X. Shu-Kun, and Z. Xiu-Juan, *Chin. J. Anal. Chem.*, 2007, **35**, 135.

8.2.4 Optical Characterization of Group 12-16 (II-VI) Semiconductor Nanoparticles by Fluorescence Spectroscopy[5]

Group 12-16 semiconductor nanocrystals when exposed to light of a particular energy absorb light to excite electrons from the ground state to the excited state, resulting in the formation of an electron-hole pair (also known as excitons). The excited electrons relax back to the ground state, mainly through radiative emission of energy in the form of photons.

Quantum dots (QD) refer to nanocrystals of semiconductor materials where the size of the particles is comparable to the natural characteristic separation of an electron-hole pair, otherwise known as the exciton Bohr radius of the material. In quantum dots, the phenomenon of emission of photons associated with the transition of electrons from the excited state to the ground state is called fluorescence.

[5]This content is available online at <http://cnx.org/content/m34656/1.1/>.

8.2.4.1 Fluorescence spectroscopy

Emission spectroscopy, in general, refers to a characterization technique that measures the emission of radiation by a material that has been excited. Fluorescence spectroscopy is one type of emission spectroscopy which records the intensity of light radiated from the material as a function of wavelength. It is a nondestructive characterization technique.

After an electron is excited from the ground state, it needs to relax back to the ground state. This relaxation or loss of energy to return to the ground state, can be achieved by a combination of non-radiative decay (loss of energy through heat) and radiative decay (loss of energy through light). Non-radiative decay by vibrational modes typically occurs between energy levels that are close to each other. Radiative decay by the emission of light occurs when the energy levels are far apart like in the case of the band gap. This is because loss of energy through vibrational modes across the band gap can result in breaking the bonds of the crystal. This phenomenon is shown in Figure 8.19.
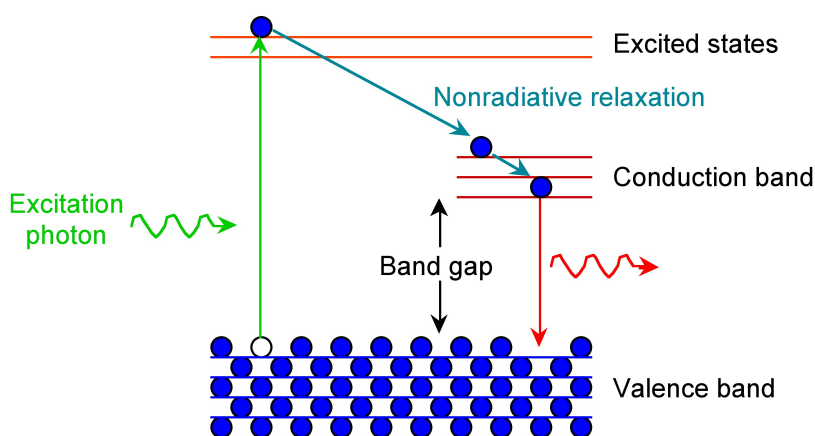
Figure 8.19: Emission of luminescence photon for Group 12-16 semiconductor quantum dot.

The band gap of Group 12-16 semiconductors is in the UV-visible region. Thus, the wavelength of the emitted light as a result of radiative decay is also in the visible region, resulting in fascinating fluorescence properties.

A fluorimeter is a device that records the fluorescence intensity as a function of wavelength. The fluorescence quantum yield can then be calculated by the ratio of photons absorbed to photons emitted by the system. The quantum yield gives the probability of the excited state getting relaxed via fluorescence rather than by any other non-radiative decay.

8.2.4.2 Difference between fluorescence and phosphorescence

Photoluminescence is the emission of light from any material due to the loss of energy from excited state to ground state. There are two main types of luminescence – fluorescence and phosphorescence. Fluorescence is a fast decay process, where the emission rate is around 10^8 s^{-1} and the lifetime is around 10^{-9} - 10^{-7} s. Fluorescence occurs when the excited state electron has an opposite spin compared to the ground state electrons. From the laws of quantum mechanics, this is an allowed transition, and occurs rapidly by emission of a photon. Fluorescence disappears as soon as the exciting light source is removed.

Phosphorescence is the emission of light, in which the excited state electron has the same spin orientation as the ground state electron. This transition is a forbidden one and hence the emission rates are slow (10^3 -

10^0 s^{-1}). So the phosphorescence lifetimes are longer, typically seconds to several minutes, while the excited phosphors slowly returned to the ground state. Phosphorescence is still seen, even after the exciting light source is removed. Group 12-16 semiconductor quantum dots exhibit fluorescence properties when excited with ultraviolet light.

8.2.4.3 Instrumentation

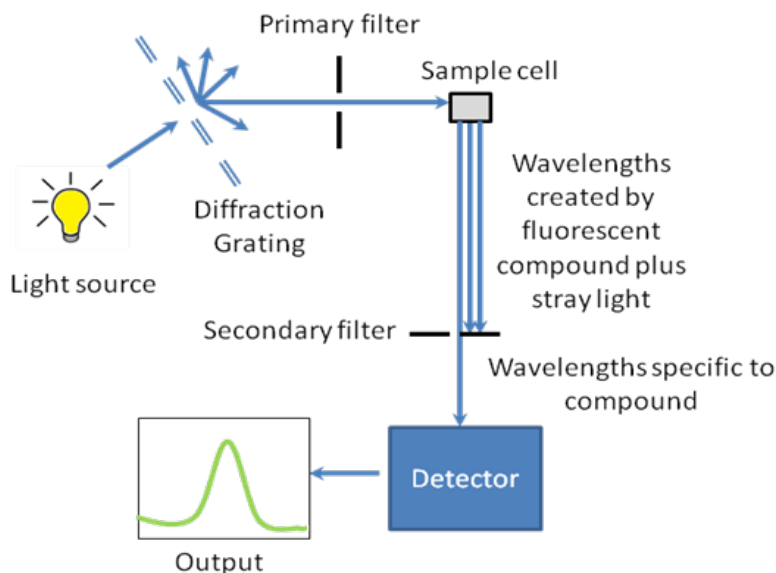The working schematic for the fluorometer is shown in Figure 8.20.

Figure 8.20: Schematic of fluorometer.

8.2.4.3.1 The light source

The excitation energy is provided by a light source that can emit wavelengths of light over the ultraviolet and the visible range. Different light sources can be used as excitation sources such as lasers, xenon arcs and mercury-vapor lamps. The choice of the light source depends on the sample. A laser source emits light of a high irradiance at a very narrow wavelength interval. This makes the need for the filter unnecessary, but the wavelength of the laser cannot be altered significantly. The mercury vapor lamp is a discrete line source. The xenon arc has a continuous emission spectrum between the ranges of 300 - 800 nm.

8.2.4.3.2 The diffraction grating and primary filter

The diffraction grating splits the incoming light source into its component wavelengths (Figure 8.20). The monochromator can then be adjusted to choose with wavelengths to pass through. Following the primary filter, specific wavelengths of light are irradiated onto the sample

8.2.4.3.3 Sample cell and sample preparation

A proportion of the light from the primary filter is absorbed by the sample. After the sample gets excited, the fluorescent substance returns to the ground state, by emitting a longer wavelength of light in all directions (Figure 8.20). Some of this light passes through a secondary filter. For liquid samples, a square cross section tube sealed at one end and all four sides clear, is used as a sample cell. The choice of cuvette depends on three factors:

1. **Type of solvent** - For aqueous samples, specially designed rectangular quartz, glass or plastic cuvettes are used. For organic samples glass and quartz cuvettes are used.
2. **Excitation wavelength** – Depending on the size and thus, bandgap of the Group 12-16 semiconductor nanoparticles, different excitation wavelengths of light are used. Depending on the excitation wavelength, different materials are used (Table 8.3).

Cuvette	Wavelength (nm)
Visible only glass	380 - 780
Visible only plastic	380 - 780
UV plastic	220 - 780
Quartz	200 - 900

Table 8.3: Cuvette materials and their wavelengths.

3. **Cost** – Plastic cuvettes are the least expensive and can be discarded after use. Though quartz cuvettes have the maximum utility, they are the most expensive, and need to reused. Generally, disposable plastic cuvettes are used when speed is more important than high accuracy.
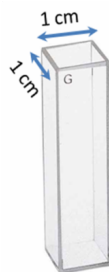
Figure 8.21: A typical cuvette for fluorescence spectroscopy.

The cuvettes have a 1 cm path length for the light (Figure 8.21). The best cuvettes need to be very clear and have no impurities that might affect the spectroscopic reading. Defects on the cuvette, such as scratches, can scatter light and hence should be avoided. Since the specifications of a cuvette are the same for both, the UV-visible spectrophotometer and fluorimeter, the same cuvette that is used to measure absorbance can be used to measure the fluorescence. For Group 12-16 semiconductor nanoparticles preparted in organic solvents, the clear four sided quartz cuvette is used. The sample solution should be dilute (absorbance <1 au), to avoid very high signal from the sample to burn out the detector. The solvent used to disperse the nanoparticles should not absorb at the excitation wavelength.

8.2.4.3.4 Secondary filter

The secondary filter is placed at a 90 ° angle (Figure 8.20) to the original light path to minimize the risk of transmitted or reflected incident light reaching the detector. Also this minimizes the amount of stray light, and results in a better signal-to-noise ratio. From the secondary filter, wavelengths specific to the sample are passed onto the detector.

8.2.4.3.5 Detector

The detector can either be single-channeled or multichanneled (Figure 8.20). The single-channeled detector can only detect the intensity of one wavelength at a time, while the multichanneled detects the intensity at all wavelengths simultaneously, making the emission monochromator or filter unnecessary. The different types of detectors have both advantages and disadvantages.

8.2.4.3.6 Output

The output is the form of a plot of intensity of emitted light as a function of wavelength as shown in Figure 8.22.
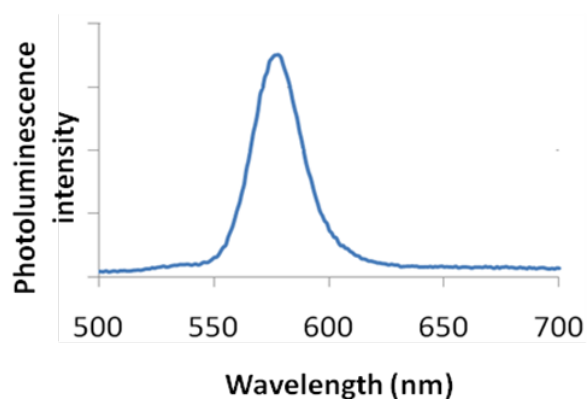
Figure 8.22: Emission spectra of CdSe quantum dot.

8.2.4.4 Analysis of data

The data obtained from fluorimeter is a plot of fluorescence intensity as a function of wavelength. Quantitative and qualitative data can be obtained by analysing this information.

8.2.4.4.1 Quantitative information

From the fluorescence intensity versus wavelength data, the quantum yield (Φ_F) of the sample can be determined. Quantum yield is a measure of the ratio of the photons absorbed with respect to the photons emitted. It is important for the application of Group 12-16 semiconductor quantum dots using their fluorescence properties, for e.g., bio-markers.

The most well-known method for recording quantum yield is the comparative method which involves the use of well characterized standard solutions. If a test sample and a standard sample have similar absorbance values at the same excitation wavelength, it can be assumed that the number of photons being absorbed by

both the samples is the same. This means that a ratio of the integrated fluorescence intensities of the test and standard sample measured at the same excitation wavelength will give a ratio of quantum yields. Since the quantum yield of the standard solution is known, the quantum yield for the unknown sample can be calculated.

A plot of integrated fluorescence intensity versus absorbance at the excitation wavelength is shown in Figure 8.23. The slope of the graphs shown in Figure 8.23 are proportional to the quantum yield of the different samples. Quantum yield is then calculated using (8.15), where subscripts ST denotes standard sample and X denotes the test sample; QY is the quantum yield; RI is the refractive index of the solvent.
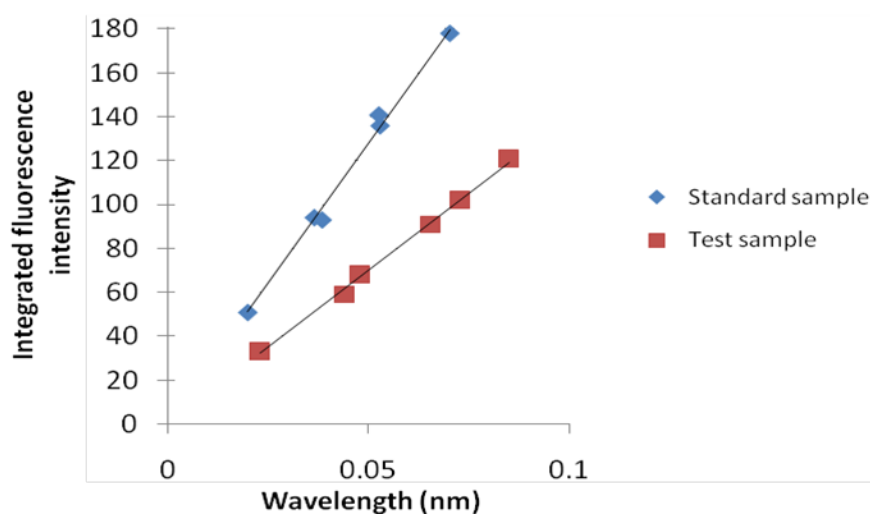

Figure 8.23: Integrated fluoresncene intensity as a function of absorbance.

$$\frac{QY_X}{QY_{ST}} = \frac{\text{slope}_X \ (RI_X)^2}{\text{slope}_{ST} \ (RI_{ST})^2} \tag{8.15}$$

Take the example of Figure 8.23. If the same solvent is used in both the sample and the standard solution, the ratio of quantum yields of the sample to the standard is given by (8.16). If the quantum yield of the standard is known to 0.95, then the quantum yield of the test sample is 0.523 or 52.3%.

$$\frac{QY_X}{QY_{ST}} = \frac{1.41}{2.56} \tag{8.16}$$

The assumption used in the comparative method is valid only in the Beer-Lambert law linear regime. Beer-Lambert law states that absorbance is directly proportional to the path length of light travelled within the sample, and concentration of the sample. The factors that affect the quantum yield measurements are the following:

- **Concentration** – Low concentrations should be used (absorbance < 0.2 a.u.) to avoid effects such as self quenching.
- **Solvent** – It is important to take into account the solvents used for the test and standard solutions. If the solvents used for both are the same then the comparison is trivial. However, if the solvents in the test and standard solutions are different, this difference needs to be accounted for. This is done by incorporating the solvent refractive indices in the ratio calculation.

- **Standard samples** – The standard samples should be characterized thoroughly. In addition, the standard sample used should absorb at the excitation wavelength of the test sample.
- **Sample preparation** – It is important that the cuvettes used are clean, scratch free and clear on all four sides. The solvents used must be of spectroscopic grade and should not absorb in the wavelength range.
- **Slit width** – The slit widths for all measurements must be kept constant.

The quantum yield of the Group 12-16 semiconductor nanoparticles are affected by many factors such as the following.

- **Surface defects** – The surface defects of semiconductor quantum dots occur in the form of unsatisfied valencies. Thus resulting in unwanted recombinations. These unwanted recombinations reduce the loss of energy through radiative decay, and thus reducing the fluorescence.
- **Surface ligands** – If the surface ligand coverage is a 100%, there is a smaller chance of surface recombinations to occur.
- **Solvent polarity** – If the solvent and the ligand have similar solvent polarities, the nanoparticles are more dispersed, reducing the loss of electrons through recombinations.

8.2.4.4.2 Qualitative Information

Apart from quantum yield information, the relationship between intensity of fluorescence emission and wavelength, other useful qualitative information such as size distribution, shape of the particle and presence of surface defects can be obtained.

As shown in Figure 8.24, the shape of the plot of intensity versus wavelength is a Gaussian distribution. In Figure 8.24, the full width at half maximum (FWHM) is given by the difference between the two extreme values of the wavelength at which the photoluminescence intensity is equal to half its maximum value. From the full width half max (FWHM) of the fluorescence intensity Gaussian distribution, it is possible to determine qualitatively the size distribution of the sample. For a Group 12-16 quantum dot sample if the FWHM is greater than 30, the system is very polydisperse and has a large size distribution. It is desirable for all practical applications for the FWHM to be lesser than 30.
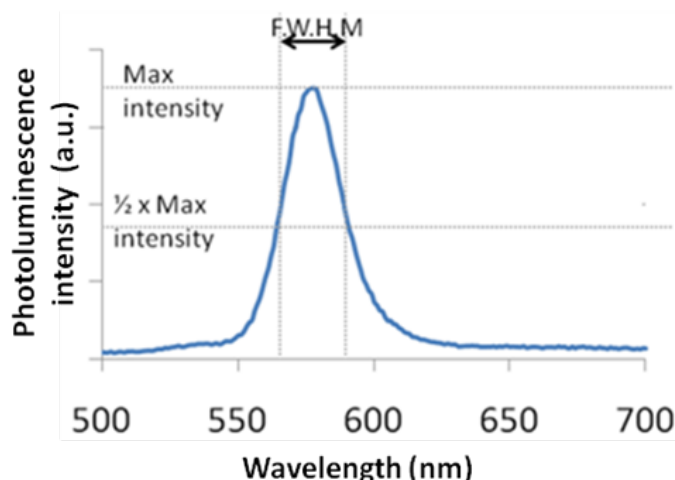
Figure 8.24: Emission spectra of CdSe QDs showing the full width half maximum (FWHM).

From the FWHM of the emission spectra, it is also possible to qualitatively get an idea if the particles are spherical or shaped. During the synthesis of the shaped particles, the thickness of the rod or the arm of the tetrapod does not vary among the different particles, as much as the length of the rods or arms changes. The thickness of the arm or rod is responsible for the quantum effects in shaped particles. In the case of quantum dots, the particle is quantum confined in all dimensions. Thus, any size distribution during the synthesis of quantum dots greatly affects the emission spectra. As a result the FWHM of rods and tetrapods is much smaller as compared to a quantum dot. Hence, qualitatively it is possible to differentiate between quantum dots and other shaped particles.

Another indication of branched structures is the decrease in the intensity of fluorescence peaks. Quantum dots have very high fluorescence values as compared to branched particles, since they are quantum confined in all dimensions as compared to just 1 or 2 dimensions in the case of branched particles.

8.2.4.5 Fluorescence spectra of different Group 12-16 semiconductor nanoparticles

The emission spectra of all Group 12-16 semiconductor nanoparticles are Gaussian curves as shown in Figure 8.22 and Figure 8.24. The only difference between them is the band gap energy, and hence each of the Group 12-16 semiconductor nanoparticles fluoresce over different ranges of wavelengths

8.2.4.5.1 Cadmium selenide

Since its bulk band gap (1.74 eV, 712 nm) falls in the visible region cadmium Selenide (CdSe) is used in various applications such as solar cells, light emitting diodes, etc. Size evolving emission spectra of cadmium selenide is shown in Figure 8.25. Different sized CdSe particles have different colored fluorescence spectra. Since cadmium and selenide are known carcinogens and being nanoparticles are easily absorbed into the human body, there is some concern regarding these particles. However, CdSe coated with ZnS can overcome all the harmful biological effects, making cadmium selenide nanoparticles one of the most popular 12-16 semiconductor nanoparticle.
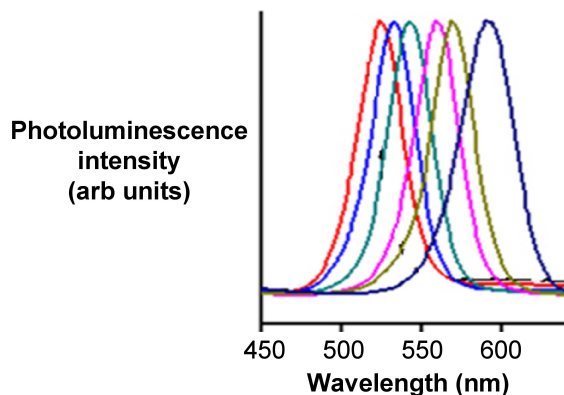
Figure 8.25: Size evolving CdSe emission spectra. Adapted from http://www.physics.mq.edu.au.

A combination of the absorbance and emission spectra is shown in Figure 8.26 for four different sized particles emitting green, yellow, orange, and red fluorescence.
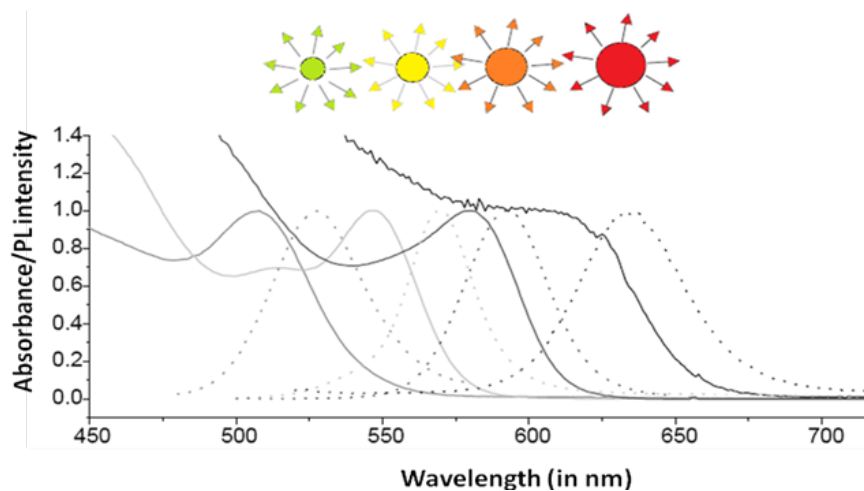
Figure 8.26: Absorption and emission spectra of CdSe quantum dots. Adapted from G. Schmid, *Nanoparticles: From Theory to Application*, Wiley-VCH, Weinham (2004).

8.2.4.5.2 Cadmium telluride

Cadmium Telluride (CdTe) has a band gap of 1.44 eV and thus absorbs in the infra red region. The size evolving CdTe emission spectra is shown in Figure 8.27.
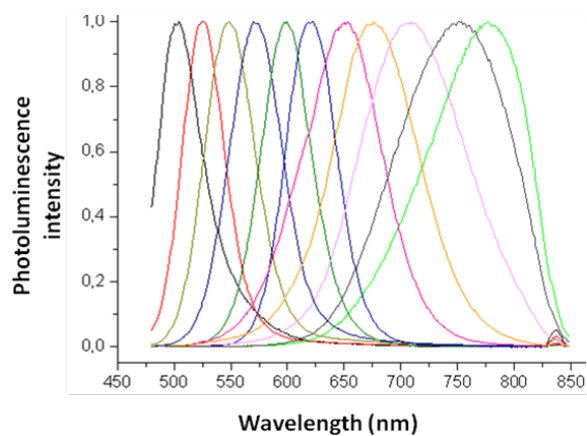
Figure 8.27: Size evolution spectra of CdTe quantum dots.

8.2.4.5.3 Adding shells to QDs

Capping a core quantum dot with a semiconductor material with a wider bandgap than the core, reduces the nonradiative recombination and results in brighter fluorescence emission. Quantum yields are affected by the presences of free surface charges, surface defects and crystal defects, which results in unwanted recombinations. The addition of a shell reduces the nonradiative transitions and majority of the electrons relax radiatively to the valence band. In addition, the shell also overcomes some of the surface defects.

For the CdSe-core/ZnS-shell systems exhibit much higher quantum yield as compared to core CdSe quantum dots as seen in Figure 8.28.
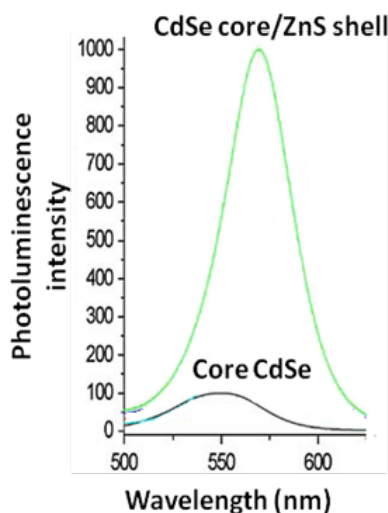

Figure 8.28: Emission spectra of core CdSe only and CdSe-core/ZnS-shell.

8.2.4.6 Bibliography

- A. T. R. Williams, S. A. Winfield, and J. N. Miller, *Analyst*, 1983, **108**, 1067.
- G. Schmid, *Nanoparticles: From Theory to Application*, Wiley-VCH, Weinham, (2004).
- J. Y. Hariba, *A Guide to Recording Fluorescence Quantum Yield*, Jobin Yvon Hariba Limited, Stanmore (2003).
- C. Qing Zhu, P. Wang, X. Wang, and Y. Li, *Nanoscale Res. Lett..*, 2008, **3**, 213.

8.3 Carbon Nanomaterials[6]

8.3.1 Introduction

Although nanomaterials had been known for many years prior to the report of C_{60} the field of nanoscale science was undoubtedly founded upon this seminal discovery. Part of the reason for this explosion in nanochemistry is that while carbon materials range from well-defined nano sized molecules (i.e., C_{60}) to tubes with lengths of hundreds of microns, they do not exhibit the instabilities of other nanomaterials as

---

[6]This content is available online at <http://cnx.org/content/m22580/1.4/>.

a result of the very high activation barriers to their structural rearrangement. As a consequence they are highly stable even in their unfunctionalized forms. Despite this range of carbon nanomaterials possible they exhibit common reaction chemistry: that of organic chemistry.

The previously unknown allotrope of carbon: C_{60}, was discovered in 1985, and in 1996, Curl, Kroto, and Smalley were awarded the Nobel Prize in Chemistry for the discovery. The other allotropes of carbon are graphite (sp^2) and diamond (sp^3). C_{60}, commonly known as the "buckyball" or "Buckminsterfullerene", has a spherical shape comprising of highly pyramidalized sp^2 carbon atoms. The C_{60} variant is often compared to the typical soccer football, hence buckyball. However, confusingly, this term is commonly used for higher derivatives. Fullerenes are similar in sheet structure to graphite but they contain pentagonal (or sometimes heptagonal) rings that prevent the sheet from being planar. The unusual structure of C_{60} led to the introduction of a new class of molecules known as fullerenes, which now constitute the third allotrope of carbon. Fullerenes are commonly defined as "any of a class of closed hollow aromatic carbon compounds that are made up of twelve pentagonal and differing numbers of hexagonal faces."

The number of carbon atoms in a fullerene range from C_{60} to C_{70}, C_{76}, and higher. Higher order fullerenes include carbon nanotubes that can be described as fullerenes that have been stretched along a rotational axis to form a tube. As a consequence of differences in the chemistry of fullerenes such as C_{60} and C_{70} as compared to nanotubes, these will be dealt with separately herein. In addition there have also been reports of nanohorns and nanofibers, however, these may be considered as variations on the general theme. It should be noted that fullerenes and nanotubes have been shown to be in flames produced by hydrocarbon combustion. Unfortunately, these naturally occurring varieties can be highly irregular in size and quality, as well as being formed in mixtures, making them unsuitable for both research and industrial applications.

8.3.2 Fullerenes

Carbon-60 (C_{60}) is probably the most studied individual type of nanomaterial. The spherical shape of C_{60} is constructed from twelve pentagons and twenty hexagons and resembles a soccer ball (Figure 8.29a). The next stable higher fullerene is C_{70} (Figure 8.29b) that is shaped like a rugby or American football. The progression of higher fullerenes continues in the sequence C_{74}, C_{76}, C_{78}, etc. The structural relationship between each involves the addition of six membered rings. Mathematically (and chemically) two principles define the existence of a stable fullerene, i.e., Euler's theorem and isolated pentagon rule (IPR). Euler's theorem states that for the closure of each spherical network, n (n $\geq$ 2) hexagons and 12 pentagons are required while the IPR says no two pentagons may be connected directly with each other as destabilization is caused by two adjacent pentagons.

(a)   (b)
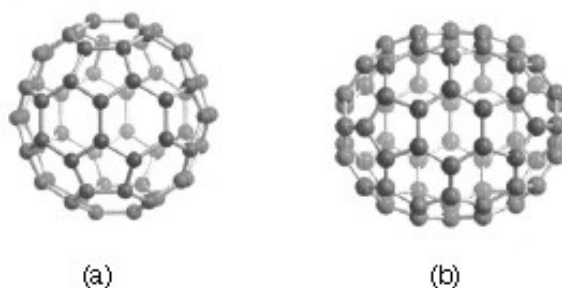
Figure 8.29: Molecular structures of (a) C_{60} and (b) C_{70}.

Although fullerenes are composed of sp^2 carbons in a similar manner to graphite, fullerenes are soluble

in various common organic solvents. Due to their hydrophobic nature, fullerenes are most soluble in CS_2 (C_{60} = 7.9 mg/mL) and toluene (C_{60} = 2.8 mg/mL). Although fullerenes have a conjugated system, their aromaticity is distinctive from benzene that has all C-C bonds of equal lengths, in fullerenes two distinct classes of bonds exist. The shorter bonds are at the junctions of two hexagons ([6, 6] bonds) and the longer bonds at the junctions of a hexagon and a pentagon ([5,6] bonds). This difference in bonding is responsible for some of the observed reactivity of fullerenes.

8.3.2.1 Synthesis of fullerenes

The first observation of fullerenes was in molecular beam experiments at Rice University. Subsequent studies demonstrated that C_{60} it was relatively easy to produce grams of fullerenes. Although the synthesis is relatively straightforward fullerene purification remains a challenge and determines fullerene's commercial price. The first method of production of measurable quantities of fullerenes used laser vaporization of carbon in an inert atmosphere, but this produced microscopic amounts of fullerenes. Laboratory scales of fullerene are prepared by the vaporization of carbon rods in a helium atmosphere. Commercial production ordinarily employs a simple ac or dc arc. The fullerenes in the black soot collected are extracted in toluene and purified by liquid chromatography. The magenta C_{60} comes off the column first, followed by the red C_{70}, and other higher fullerenes. Even though the mechanism of a carbon arc differs from that of a resistively heated carbon rod (because it involves a plasma) the He pressure for optimum C_{60} formation is very similar.

A ratio between the mass of fullerenes and the total mass of carbon soot defines fullerene yield. The yields determined by UV-Vis absorption are approximately 40%, 10-15%, and 15% in laser, electric arc, and solar processes. Interestingly, the laser ablation technique has both the highest yield and the lowest productivity and, therefore, a scale-up to a higher power is costly. Thus, fullerene commercial production is a challenging task. The world's first computer controlled fullerene production plant is now operational at the MER Corporation, who pioneered the first commercial production of fullerene and fullerene products.

8.3.2.2 Endohedral fullerenes

Endohedral fullerenes are fullerenes that have incorporated in their inner sphere atoms, ions or clusters. Endohedral fullerenes are generally divided into two groups: endohedral metallofullerenes and non-metal doped fullerenes. The first endohedral metallofullerenes was called La@C_{60}. The @ sign in the name reflects the notion of a small molecule trapped inside a shell.

Doping fullerenes with metals takes place *in-situ* during the fullerene synthesis in an arc reactor or via laser evaporation. A wide range of metals have been encased inside a fullerene, i.e., Sc, Y, La, Ce, Ba, Sr, K, U, Zr, and Hf. Unfortunately, the synthesis of endohedral metallofullerenes is unspecific because in addition a high yield of unfilled fullerenes, compounds with different cage sizes are prepared (e.g., La@C_{60} or La@C_{82}). A characteristic of endohedral metallofullerenes is that electrons will transfer from the metal atom to the fullerene cage and that the metal atom takes a position off-center in the cage. The size of the charge transfer is not always simple to determine, but it is usually between 2 and 3 units (e.g., La$_2$@C_{80}) but can be as high as 6 electrons (e.g., Sc$_3$N@C_{80}). These anionic fullerene cages are very stable molecules and do not have the reactivity associated with ordinary empty fullerenes (see below). This lack of reactivity is utilized in a method to purify endohedral metallofullerenes from empty fullerenes.

The endohedral He@C_{60} and Ne@C_{60} form when C_{60} is exposed to a pressure of around 3 bar of the appropriate noble gases. Under these conditions it was possible to dope 1 in every 650,000 C_{60} cages with a helium atom. Endohedral complexes with He, Ne, Ar, Kr and Xe as well as numerous adducts of the He@C_{60} compound have also been proven with operating pressures of 3000 bars and incorporation of up to 0.1 % of the noble gases. The isolation of N@C_{60}, N@C_{70} and P@C_{60} is very unusual and unlike the metal derivatives no charge transfer of the pnictide atom in the center to the carbon atoms of the cage takes place.

8.3.2.3 Chemically functionalized fullerenes

Although fullerenes have a conjugated aromatic system all the carbons are quaternary (i.e., containing no hydrogen), which results in making many of the characteristic substitution reactions of planar aromatics impossible. Thus, only two types of chemical transformations exist: redox reactions and addition reactions. Of these, addition reactions have the largest synthetic value. Another remarkable feature of fullerene addition chemistry is the thermodymics of the process. Since the sp^2 carbon atoms in a fullerene are paramidalized there is significant strain energy. For example, the strain energy in C_{60} is *ca* 8 kcal/mol, which is 80% of its heat of formation. So the relief of this strain energy leading to sp^3 hybridized C atoms is the major driving force for addition reactions (Figure 8.30). As a consequence, most additions to fullerenes are exothermic reactions.
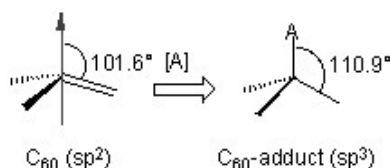

Figure 8.30: Strain release after addition of reagent A to a pyramidalize carbon of C_{60}.

Cyclic voltammetry (CV) studies show that C_{60} can be reduced and oxidized reversibly up to 6 electrons with one-electron transfer processes. Fulleride anions can be generated by electrochemical method and then be used to synthesize covalent organofullerene derivatives. Alkali metals can chemically reduce fullerene in solution and solid state to form $M_x C_{60}$ (x = 3 - 6). C_{60} can also be reduced by less electropositive metals like mercury to form C_{60}^- and C_{60}^{2-}. In addition, salts can also be synthesized with organic molecules, for example $[TDAE^+][C_{60}^-]$ possesses interesting electronic and magnetic behavior.

Geometric and electronic analysis predicted that fullerene behaves live an electro-poor conjugated polyolefin. Indeed C_{60} and C_{70} undergo a range of nucleophilic reactions with carbon, nitrogen, phosphorous and oxygen nucleophiles. C60 reacts readily with organolithium and Grignard compounds to form alkyl, phenyl or alkanyl fullerenes. Possibly the most widely used additions to fullerene is the Bingel reaction (Figure 8.31), where a carbon nucleophile, generated by deprotonation of α-halo malonate esters or ketones, is added to form a cyclopropanation product. The α-halo esters and ketones can also be generated in situ with I_2 or CBr_4 and a weak base as 1,8-diazabicyclo[5.4.0]unde-7ene (DBU). The Bingel reaction is considered one of the most versatile and efficient methods to functionalize C_{60}.
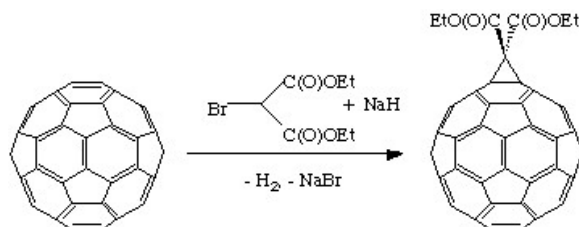

Figure 8.31: Bingel reaction of C_{60} with 2-bromoethylmalonate.

Cycloaddition is another powerful tool to functionalize fullerenes, in particular because of its selectivity with the 6,6 bonds, limiting the possible isomers (Figure 8.32). The dienophilic feature of the [6,6] double bonds of C_{60} enables the molecule to undergo various cycloaddition reactions in which the monoadducts can be generated in high yields. The best studies cycloadditon reactions of fullerene are [3+2] additions with diazoderivatives and azomethine ylides (Prato reactions). In this reaction, azomethine ylides can be generated *in situ* from condensation of α-amino acids with aldehydes or ketones, which produce 1,3 dipoles to further react with C_{60} in good yields (Figure 8.33). Hundreds of useful building blocks have been generated by those two methods. The Prato reactions have also been successfully applied to carbon nanotubes.
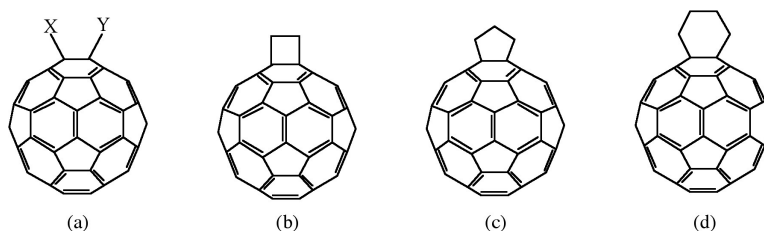
Figure 8.32: Geometrical shapes built onto a [6,6] ring junction: a) open, b) four-membered ring, c) five-membered ring, and d) six-membered ring.
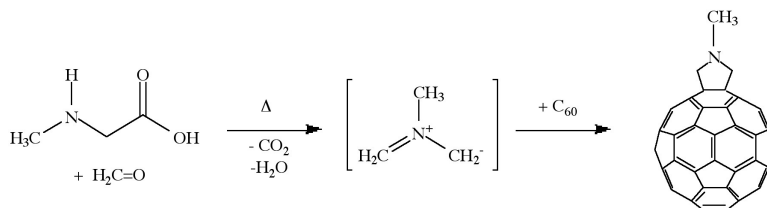
**Figure 8.33:** Prato reaction of C_{60} with N-methyglycine and paraformaldehyde.

The oxidation of fullerenes, such as C_{60}, has been of increasing interest with regard to applications in photoelectric devices, biological systems, and possible remediation of fullerenes. The oxidation of C_{60} to $C_{60}O_n$ (n = 1, 2) may be accomplished by photooxidation, ozonolysis, and epoxidation. With each of these methods, there is a limit to the isolable oxygenated product, $C_{60}O_n$ with n < 3. Highly oxygenated fullerenes, $C_{60}O_n$ with $3 \leq n \leq 9$, have been prepared by the catalytic oxidation of C_{60} with $ReMeO_3/H_2O_2$.

8.3.3 Carbon nanotubes

A key breakthrough in carbon nanochemistry came in 1993 with the report of needle-like tubes made exclusively of carbon. This material became known as carbon nanotubes (CNTs). There are several types of nanotubes. The first discovery was of multi walled tubes (MWNTs) resembling many pipes nested within each other. Shortly after MWNTs were discovered single walled nanotubes (SWNTs) were observed. Single walled tubes resemble a single pipe that is potentially capped at each end. The properties of single walled

and multi walled tubes are generally the same, although single walled tubes are believed to have superior mechanical strength and thermal and electrical conductivity; it is also more difficult to manufacture them.

Single walled carbon nanotubes (SWNTs) are by definition fullerene materials. Their structure consists of a graphene sheet rolled into a tube and capped by half a fullerene (Figure 8.34). The carbon atoms in a SWNT, like those in a fullerene, are sp2 hybridized. The structure of a nanotube is analogous to taking this graphene sheet and rolling it into a seamless cylinder. The different types of SWNTs are defined by their diameter and chirality. Most of the presently used single-wall carbon nanotubes have been synthesized by the pulsed laser vaporization method, however, increasingly SWNTs are prepared by vapor liquid solid catalyzed growth.
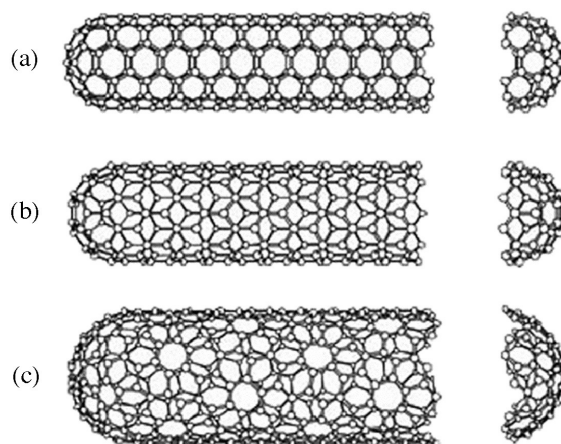

Figure 8.34: Structure of single walled carbon nanotubes (SWNTs) with (a) armchair, (b) zig-zag, and (c) chiral chirality.

The physical properties of SWNTs have made them an extremely attractive material for the manufacturing of nano devices. SWNTs have been shown to be stronger than steel as estimates for the Young's modulus approaches 1 Tpa. Their electrical conductance is comparable to copper with anticipate current densities of up to 10^{13} A/cm^2 and a resistivity as low as 0.34 x 10^{-4} Ω.cm at room temperatures. Finally, they have a high thermal conductivity (3000 - 6000 W.m/K).

The electronic properties of a particular SWNT structure are based on its chirality or twist in the structure of the tube which is defined by its *n,m* value. The values of *n* and *m* determine the chirality, or "twist" of the nanotube. The chirality in turn affects the conductance of the nanotube, its density, its lattice structure, and other properties. A SWNT is considered metallic if the value *n-m* is divisible by three. Otherwise, the nanotube is semi-conducting. The external environment also has an effect on the conductance of a tube, thus molecules such as O_2 and NH_3 can change the overall conductance of a tube, while the presence of metals have been shown to significantly effect the opto-electronic properties of SWNTs.

Multi walled carbon nanotubes (MWNTs) range from double walled NTs, through many-walled NTs (Figure 8.35) to carbon nanofibers. Carbon nanofibers are the extreme of multi walled tubes (Figure 8.36) and they are thicker and longer than either SWNTs or MWNTs, having a cross-sectional of ca. 500 Å^2 and are between 10 to 100 μm in length. They have been used extensively in the construction of high strength composites.
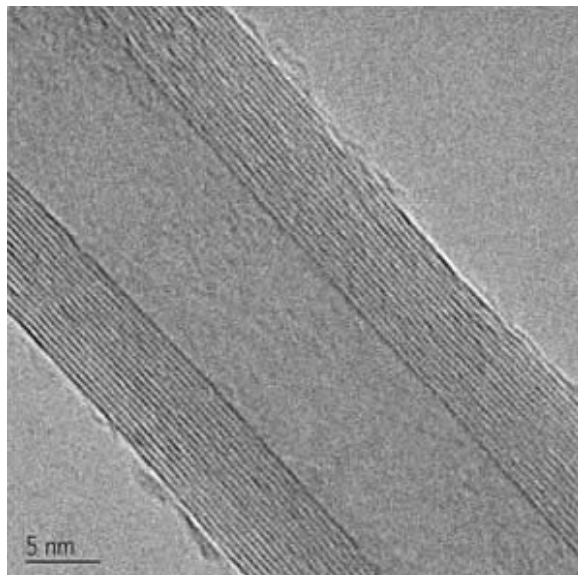
Figure 8.35: TEM image of an individual multi walled carbon nanotube (MWNTs). Copyright of Nanotech Innovations.
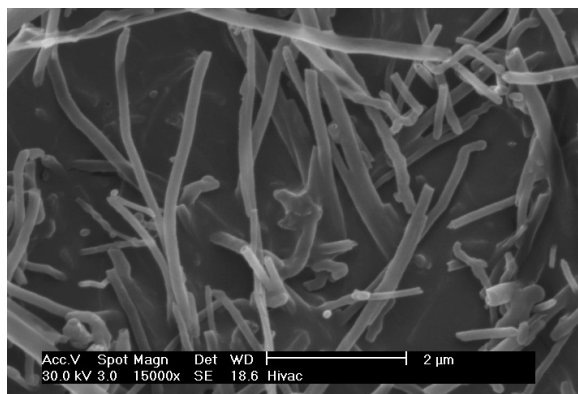
Figure 8.36: SEM image of vapor grown carbon nanofibers.

8.3.3.1 Synthesis of carbon nanotubes

A range of methodologies have been developed to produce nanotubes in sizeable quantities, including arc discharge, laser ablation, high pressure carbon monoxide (HiPco), and vapor liquid solid (VLS) growth. All

these processes take place in vacuum or at low pressure with a process gases, although VLS growth can take place at atmospheric pressure. Large quantities of nanotubes can be synthesized by these methods; advances in catalysis and continuous growth processes are making SWNTs more commercially viable.

The first observation of nanotubes was in the carbon soot formed during the arc discharge production of fullerenes. The high temperatures caused by the discharge caused the carbon contained in the negative electrode to sublime and the CNTs are deposited on the opposing electrode. Tubes produced by this method were initially multi walled tubes (MWNTs). However, with the addition of cobalt to the vaporized carbon, it is possible to grow single walled nanotubes. This method it produces a mixture of components, and requires further purification to separate the CNTs from the soot and the residual catalytic metals. Producing CNTs in high yield depends on the uniformity of the plasma arc, and the temperature of the deposit forming on the carbon electrode.

Higher yield and purity of SWNTs may be prepared by the use of a dual-pulsed laser. SWNTs can be grown in a 50% yield through direct vaporization of a Co/Ni doped graphite rod with a high-powered laser in a tube furnace operating at 1200 °C. The material produced by this method appears as a mat of "ropes", 10 - 20 nm in diameter and up to 100 μm or more in length. Each rope consists of a bundle of SWNTs, aligned along a common axis. By varying the process parameters such as catalyst composition and the growth temperature, the average nanotube diameter and size distribution can be varied. Although arc-discharge and laser vaporization are currently the principal methods for obtaining small quantities of high quality SWNTs, both methods suffer from drawbacks. The first is that they involve evaporating the carbon source, making scale-up on an industrial level difficult and energetically expensive. The second issue relates to the fact that vaporization methods grow SWNTs in highly tangled forms, mixed with unwanted forms of carbon and/or metal species. The SWNTs thus produced are difficult to purify, manipulate, and assemble for building nanotube-device architectures for practical applications.

In order to overcome some of the difficulties of these high-energy processes, the chemical catalysis method was developed in which a hydrocarbon feedstock is used in combination with a metal catalyst. The catalyst is typically, but not limited to iron, colbalt, or iron/molybdenum, it is heated under reducing conditions in the presence of a suitable carbon feedstock, e.g., ethylene. This method can be used for both SWNTs and MWNTs; the formation of each is controlled by the identity of the catalyst and the reaction conditions. A convenient laboratory scale apparatus is available from Nanotech Innovations, Inc., for the synthesis of highly uniform, consistent, research sample that uses pre-weighed catalyst/carbon source ampoules. This system, allows for 200 mg samples of MWNTs to be prepared for research and testing. The use of CO as a feedstock, in place of a hydrocarbon, led to the development of the high-pressure carbon monoxide (HiPco) procedure for SWNT synthesis. By this method, it is possible to produce gram quantities of SWNTs, unfortunately, efforts to scale beyond that have not met with complete success.

Initially developed for small-scale investigations of catalyst activity, vapor liquid solid (VLS) growth of nanotubes has been highly studied, and now shows promise for large-scale production of nanotubes. Recent approaches have involved the use of well-defined nanoparticle or molecular precursors and many different transition metals have been employed, but iron, nickel, and cobalt remain to be the focus of most research. The nanotubes grow at the sites of the metal catalyst; the carbon-containing gas is broken apart at the surface of the catalyst particle, and the carbon is transported to the edges of the particle, where it forms the nanotube. The length of the tube grown in surface supported catalyst VLS systems appears to be dependent on the orientation of the growing tube with the surface. By properly adjusting the surface concentration and aggregation of the catalyst particles it is possible to synthesize vertically aligned carbon nanotubes, i.e., as a carpet perpendicular to the substrate.

Of the various means for nanotube synthesis, the chemical processes show the greatest promise for industrial scale deposition in terms of its price/unit ratio. There are additional advantages to the VLS growth, which unlike the other methods is capable of growing nanotubes directly on a desired substrate. The growth sites are controllable by careful deposition of the catalyst. Additionally, no other growth methods have been developed to produce vertically aligned SWNTs.

8.3.3.2 Chemical functionalization of carbon nanotubes

The limitation of using carbon nanotubes in any practical applications has been its solubility; for example SWNTs have little to no solubility in most solvent due to the aggregation of the tubes. Aggregation/roping of nanotubes occurs as a result of the high van der Waals binding energy of *ca.* 500 eV per mm of tube contact. The van der Waals force between the tubes is so great, that it take tremendous energy to pry them apart, making it very to make combination of nanotubes with other materials such as in composite applications. The functionalization of nanotubes, i.e., the attachment of "chemical functional groups" provides the path to overcome these barriers. Functionalization can improve solubility as well as processibility, and has been used to align the properties of nanotubes to those of other materials. The clearest example of this is the ability to solubilize nanotubes in a variety of solvents, including water. It is important when discussing functionalization that a distinction is made between covalent and non-covalent functionalization.

Current methods for solubilizing nanotubes without covalent functionalization include highly aromatic solvents, super acids, polymers, or surfactants. Non-covalent "functionalization" is generally on the concept of supramolecular interactions between the SWNT and some macromolecule as a result of various adsorption forces, such as van der Waals' and π-stacking interactions. The chemical speciation of the nanotube itself is not altered as a result of the interaction. In contrast, covalent functionalization relies on the chemical reaction at either the sidewall or end of the SWNT. As may be expected the high aspect ratio of nanotubes means that sidewall functionalization is much more important than the functionalization of the cap. Direct covalent sidewall functionalization is associated with a change of hybridization from sp^2 to sp^2 and a simultaneous loss of conjugation. An alternative approach to covalent functionalization involves the reaction of defects present (or generated) in the structure of the nanotube. Defect sites can be the open ends and holes in the sidewalls, and pentagon and heptagon irregularities in the hexagon graphene framework (often associated with bends in the tubes). All these functionalizations are exohedral derivatizations. Taking the hollow structure of nanotubes into consideration, endohedral functionalization of SWNTs is possible, i.e., the filling of the tubes with atoms or small molecules. It is important to note that covalent functionalization methods have one problem in common: extensive covalent functionalization modifies SWNT properties by disrupting the continuous π-system of SWNTs.

Various applications of nanotubes require different, specific modification to achieve desirable physical and chemical properties of nanotubes. In this regard, covalent functionalization provides a higher degree of fine-tuning the chemistry and physics of SWNTs than non-covalent functionalization. Until now, a variety of methods have been used to achieve the functionalization of nanotubes (Figure 8.37).
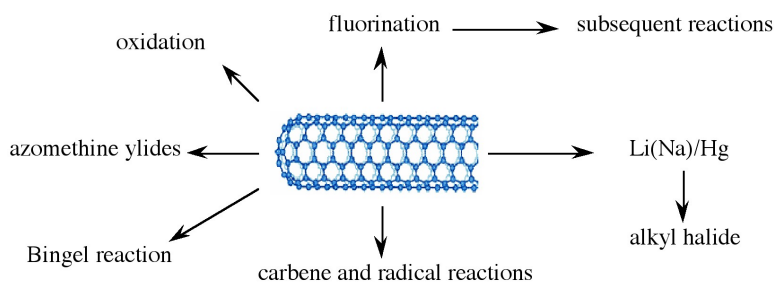

Figure 8.37: Schematic description of various covalent functionalization strategies for SWNTs.

Taking chemistry developed for C_{60}, SWNTs may be functionalized using 1,3 dipolar addition of azomethine ylides. The functionalized SWNTs are soluble in most common organic solvents. The azomethine ylide functionalization method was also used for the purification of SWNTs. Under electrochemical conditions, aryl

diazonium salts react with SWNTs to achieve functionalized SWNTs, alternatively the diazonium ions may be generated *in-situ* from the corresponding aniline, while a solvent free reaction provides the best chance for large-scale functionalization this way. In each of these methods it is possible to control the amount of functionalization on the tube by varying reaction times and the reagents used; functionalization as high as 1 group per every 10 - 25 carbon atoms is possible.

Organic functionalization through the use of alkyl halides, a radical pathway, on tubes treated with lithium in liquid ammonia offers a simple and flexible route to a range of functional groups. In this reaction, functionalization occurs on every 17 carbons. Most success has been found when the tubes are dodecylated. These tubes are soluble in chloroform, DMF, and THF.

The addition of oxygen moieties to SWNT sidewalls can be achieved by treatment with acid or wet air oxidation, and ozonolysis. The direct epoxidation of SWNTs may be accomplished by the direct reaction with a peroxide reagent, or catalytically. Catalytic de-epoxidation (Figure 8.38) allows for the quantitative analysis of sidewall epoxide and led to the surprising result that previously assumed "pure" SWNTs actually contain *ca.* 1 oxygen per 250 carbon atoms.
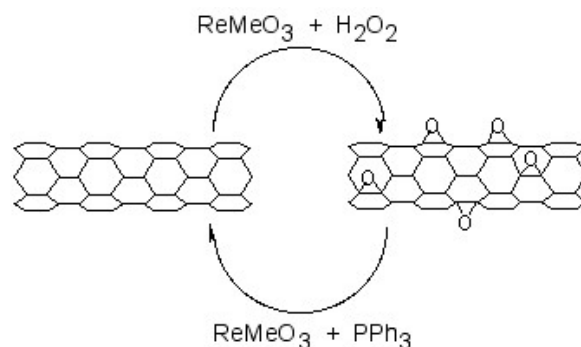
Figure 8.38: Catalytic oxidation and de-epoxidation of SWNTs.

One of the easiest functionalization routes, and a useful synthon for subsequent conversions, is the fluorination of SWNTs, using elemental fluorine. Importantly, a C:F ratios of up to 2:1 can be achieved without disruption of the tubular structure. The fluorinated SWNTs (F-SWNTs) proved to be much more soluble than pristine SWNTs in alcohols (1 mg/mL in *iso*-propanol), DMF and other selected organic solvents. Scanning tunneling microscopy (STM) revealed that the fluorine formed bands of approximately 20 nm, while calculations using DFT revealed 1,2 addition is more energetically preferable than 1,4 addition, which has been confirmed by solid state ^{13}C NMR. F-SWNTs make highly flexible synthons and subsequent elaboration has been performed with organo lithium, Grignard reagents, and amines.

Functionalized nanotubes can be characterized by a variety of techniques, such as atomic force microscopy (AFM), transmission electron microscopy (TEM), UV-vis spectroscopy, and Raman spectroscopy. Changes in the Raman spectrum of a nanotube sample can indicate if functionalization has occurred. Pristine tubes exhibit two distinct bands. They are the radial breathing mode (230 cm^{-1}) and the tangential mode (1590 cm^{-1}). When functionalized, a new band, called the disorder band, appears at *ca.*1350 cm^{-1}. This band is attributed to sp[3]-hybridized carbons in the tube. Unfortunately, while the presence of a significant D mode is consistent with sidewall functionalization and the relative intensity of D (disorder) mode versus the tangential G mode ($1550 - 1600$ cm[-1]) is often used as a measure of the level of substitution. However, it has been shown that Raman is an unreliable method for determination of the extent of functionalization since the relative intensity of the D band is also a function of the substituents distribution as well as concentration.

Recent studies suggest that solid state ^{13}C NMR are possibly the only definitive method of demonstrating covalent attachment of particular functional groups.

8.3.3.3 Coating carbon nanotubes: creating inorganic nanostructures

Fullerenes, nanotubes and nanofibers represent suitable substrates for the seeding other materials such as oxides and other minerals, as well as semiconductors. In this regard, the carbon nanomaterial acts as a seed point for the growth as well as a method of defining unusual aspect ratios. For example, silica fibers can be prepared by a number of methods, but it is only through coating SWNTs that silica nano-fibers with of micron lengths with tens of nanometers in diameter may be prepared.

While C_{60} itself does not readily seed the growth of inorganic materials, liquid phase deposition of oxides, such as silica, in the presence of fullerenol, $C_{60}(OH)_n$, results in the formation of uniform oxide spheres. It appears the fullerenol acts as both a reagent and a physical point for subsequent oxide growth, and it is C_{60}, or an aggregate of C_{60}, that is present within the spherical particle. The addition of fullerenol alters the morphology and crystal phase of $CaCO_3$ precipitates from aqueous solution, resulting in the formation of spherical features, 5-pointed flower shaped clusters, and triangular crystals as opposed to the usual rhombic crystals. In addition, the meta-stable vaterite phase is observed with the addition of $C_{60}(OH)_n$.

As noted above individual SWNTs may be obtained in solution when encased in a cylindrical micelle of a suitable surfactant. These individualized nanotubes can be coated with a range of inorganic materials. Liquid phase deposition (LPD) appears to have significant advantages over other methods such as incorporating surfaced SWNTs into a preceramic matrix, *in situ* growth of the SWNT in an oxide matrix, and sol-gel methods. The primary advantage of LPD growth is that individual SWNTs may be coated rather than bundles or ropes. For example, SWNTs have been coated with silica by liquid phase deposition (LPD) using a silica/H_2SiF_6 solution and a surfactant-stabilized solution of SWNTs. The thickness of the coating is dependent on the reaction mixture concentration and the reaction time. The SWNT core can be removed by thermolysis under oxidizing conditions to leave a silica nano fiber. It is interesting to note that the use of a surfactant is counter productive when using MWNTs and VGFs, in this case surface activation of the nanotube offers the suitable growth initiation. Pre-oxidation of the MWNT or VGF allows for uniform coatings to be deposited. The coated SWNTs, MWNTs, and VGFs can be subsequently reacted with suitable surface reagents to impart miscibility in aqueous solutions, guar gels, and organic matrixes. In addition to simple oxides, coated nanotubes have been prepared with minerals such as carbonates and semiconductors.

8.3.4 Bibliography

- S. M. Bachilo, M. S. Strano, C. Kittrell, R. H. Hauge, R. E. Smalley, and R. B. Weisman, *Science*, 2002, **298**, 2361.
- D. S. Bethune, C. H. Klang, M. S. deVries, G. Gorman, R. Savoy, J. Vazquez, and R. Beyers, *Nature*, 1993, **363**, 605.
- J, J. Brege, C. Gallaway, and A. R. Barron, *J. Phys. Chem., C*, 2007, **111**, 17812.
- C. A. Dyke and J. M. Tour, *J. Am. Chem. Soc.*, 2003, **125**, 1156.
- Z. Ge, J. C. Duchamp, T. Cai, H. W. Gibson, and H. C. Dorn, *J. Am. Chem. Soc.*, 2005, **127**, 16292.
- L. A. Girifalco, M. Hodak, and R. S. Lee, *Phys. Rev. B*, 2000, **62**, 13104.
- T. Guo, P. Nikolaev, A. G. Rinzler, D. Tománek, D. T. Colbert, and R. E. Smalley, *J. Phys. Chem.*, 1995, **99**, 10694.
- J. H. Hafner, M. J. Bronikowski, B. R. Azamian, P. Nikolaev, A. G. Rinzler, D. T. Colbert, K. A. Smith, and R. E. Smalley, *Chem. Phys. Lett.*, 1998, **296**, 195.
- A. Hirsch, *Angew. Chem. Int. Ed.*, 2002, **40**, 4002.
- S. Iijima and T. Ichihashi, *Nature*, 1993, **363**, 603.
- H. R. Jafry, E. A. Whitsitt, and A. R. Barron, *J. Mater. Sci.*, 2007, **42**, 7381.
- H. W. Kroto, J. R. Heath, S. C. O'Brien, R. F. Curl, and R. E. Smalley, *Nature*, 1985, **318**, 162.
- F. Liang, A. K. Sadana, A. Peera, J. Chattopadhyay, Z. Gu, R. H. Hauge, and W. E. Billups, *Nano Lett.*, 2004, **4**, 1257.

- D. Ogrin and A. R. Barron, *J. Mol. Cat. A: Chem.*, 2006, **244**, 267.
- D. Ogrin, J. Chattopadhyay, A. K. Sadana, E. Billups, and A. R. Barron, *J. Am. Chem. Soc.*, 2006, **128**, 11322.
- R. E. Smalley, *Acc. Chem. Res.*, 1992, **25**, 98.
- M. M. J. Treacy, T. W. Ebbesen, and J. M. Gibson, *Nature*, 1996, **381**, 678.
- E. A. Whitsitt and A. R. Barron, *Nano Lett.*, 2003, **3**, 775.
- J. Yang and A. R. Barron, *Chem. Commun.*, 2004, 2884.
- L. Zeng, L. B. Alemany, C. L. Edwards, and A. R. Barron, *Nano Res.*, 2008, **1**, 72.

8.4 Graphene[7]

8.4.1 Introduction

Graphene is a one-atom-thick planar sheet of sp^2-bonded carbon atoms that are densely packed in a honeycomb crystal lattice (Figure 8.39). The name comes from "graphite" and "alkene"; graphite itself consists of many graphene sheets stacked together.
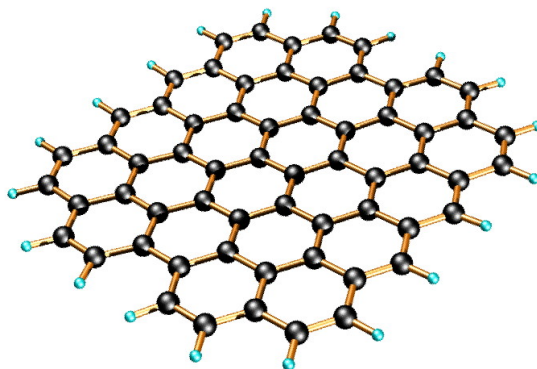
Figure 8.39: Idealized structure of a single graphene sheet.

Single-layer graphene nanosheets were first characterized in 2004, prepared by mechanical exfoliation (the "scotch-tape" method) of bulk graphite. Later graphene was produced by epitaxial chemical vapor deposition on silicon carbide and nickel substrates. Most recently, graphene nanoribbons (GNRs) have been prepared by the oxidative treatment of carbon nanotubes and by plasma etching of nanotubes embedded in polymer films.

8.4.2 Physical properties of graphene

Graphene has been reported to have a Young's modulus of 1 TPa and intrinsic strength of 130 GP; similar to single walled carbon nanotubes (SWNTs). The electronic properties of graphene also have some similarity with carbon nanotubes. Graphene is a zero-bandgap semiconductor. Electron mobility in graphene is extraordinarily high (15,000 cm^2/V.s at room temperature) and ballistic electron transport is reported to

---

[7]This content is available online at <http://cnx.org/content/m29187/1.4/>.

be on length scales comparable to that of SWNTs. One of the most promising aspects of graphene involves the use of GNRs. Cutting an individual graphene layer into a long strip can yield semiconducting materials where the bandgap is tuned by the width of the ribbon.

While graphene's novel electronic and physical properties guarantee this material will be studied for years to come, there are some fundamental obstacles yet to overcome before graphene based materials can be fully utilized. The aforementioned methods of graphene preparation are effective; however, they are impractical for large-scale manufacturing. The most plentiful and inexpensive source of graphene is bulk graphite. Chemical methods for exfoliation of graphene from graphite provide the most realistic and scalable approach to graphene materials.

Graphene layers are held together in graphite by enormous van der Waals forces. Overcoming these forces is the major obstacle to graphite exfoliation. To date, chemical efforts at graphite exfoliation have been focused primarily on intercalation, chemical derivatization, thermal expansion, oxidation-reduction, the use of surfactants, or some combination of these.

8.4.3 Graphite oxide

Probably the most common route to graphene involves the production of graphite oxide (GO) by extremely harsh oxidation chemistry. The methods of Staudenmeier or Hummers are most commonly used to produce GO, a highly exfoliated material that is dispersible in water. The structure of GO has been the subject of numerous studies; it is known to contain epoxide functional groups along the basal plane of sheets as well as hydroxyl and carboxyl moieties along the edges (Figure 8.40). In contrast to other methods for the synthesis of GO, the the m-peroxybenzoic acid (m-CPBA) oxidation of microcrystalline synthetic graphite at room temperature yields graphite epoxide in high yield, without significant additional defects.
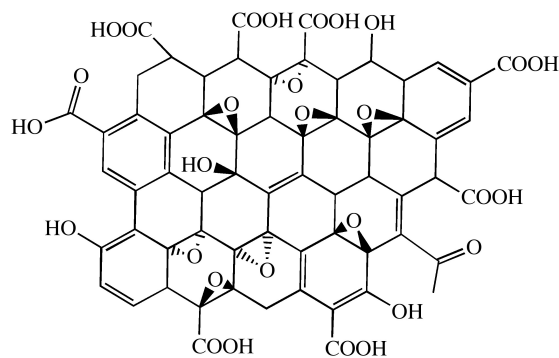
Figure 8.40: Idealized structure proposed for graphene oxide (GO). Adapted from C. E. Hamilton, PhD Thesis, Rice University (2009).

As graphite oxide is electrically insulating, it must be converted by chemical reduction to restore the electronic properties of graphene. Chemically converted graphene (CCG) is typically reduced by hydrazine or borohydride. The properties of CCG can never fully match those of graphene for two reasons:

1. Oxidation to GO introduces defects.
2. Chemical reduction does not fully restore the graphitic structure.

As would be expected, CCG is prone to aggregation unless stabilized. Graphene materials produced from pristine graphite avoid harsh oxidation to GO and subsequent (incomplete) reduction; thus, materials produced are potentially much better suited to electronics applications.

A catalytic approach to the removal of epoxides from fullerenes and SWNTs has been applied to graphene epoxide and GO. Treatment of oxidized graphenes with methyltrioxorhenium (MeReO$_3$, MTO) in the presence of PPh$_3$ results in the oxygen transfer, to form O=PPh$_3$ and allow for quantification of the C:O ratio.

8.4.4 Homogeneous graphene dispersions

An alternate approach to producing graphene materials involves the use of pristine graphite as starting material. The fundamental value of such an approach lies in its avoidance of oxidation to GO and subsequent (incomplete) reduction, thereby preserving the desirable electronic properties of graphene. There is precedent for exfoliation of pristine graphite in neat organic solvents without oxidation or surfactants. It has been reported that N,N-dimethylformamide (DMF) dispersions of graphene are possible, but no detailed characterization of the dispersions were reported. In contrast, Coleman and coworkers reported similar dispersions using N-methylpyrrolidone (NMP), resulting in individual sheets of graphene at a concentration of ≤0.01 mg/mL. NMP and DMF are highly polar solvents, and not ideal in cases where reaction chemistry requires a nonpolar medium. Further, they are hygroscopic, making their use problematic when water must be excluded from reaction mixtures. Finally, DMF is prone to thermal and chemical decomposition.

Recently, dispersions of graphene has been reported in *ortho*-dichlorobenzene (ODCB) using a wide range of graphite sources. The choice of ODCB for graphite exfoliation was based on several criteria:

1. ODCB is a common reaction solvent for fullerenes and is known to form stable SWNT dispersions.
2. ODCB is a convenient high-boiling aromatic, and is compatible with a variety of reaction chemistries.
3. ODCB, being aromatic, is able to interact with graphene *via* π-π stacking.
4. It has been suggested that good solvents for graphite exfoliation should have surface tension values of $40-50$ mJ/m^2. ODCB has a surface tension of 36.6 mJ/m^2, close to the proposed range.

Graphite is readily exfoliated in ODCB with homogenization and sonication. Three starting materials were successfully dispersed: microcrystalline synthetic, thermally expanded, and highly ordered pyrolytic graphite (HOPG). Dispersions of microcrystalline synthetic graphite have a concentration of 0.03 mg/mL, determined gravimetrically. Dispersions from expanded graphite and HOPG are less concentrated (0.02 mg/mL).

High resolution transmission electron microscopy (HRTEM) shows mostly few-layer graphene (n < 5) with single layers and small flakes stacked on top (Figure 8.41). Large graphitic domains are visible; this is further supported by selected area electron diffraction (SAED) and fast Fourier transform (FFT) in selected areas. Atomic force microscope (AFM) images of dispersions sprayed onto silicon substrates shows extremely thin flakes with nearly all below 10 nm. Average height is 7 - 10 nm. The thinnest are less than 1 nm, graphene monolayers. Lateral dimensions of nanosheets range from $100-500$ nm.
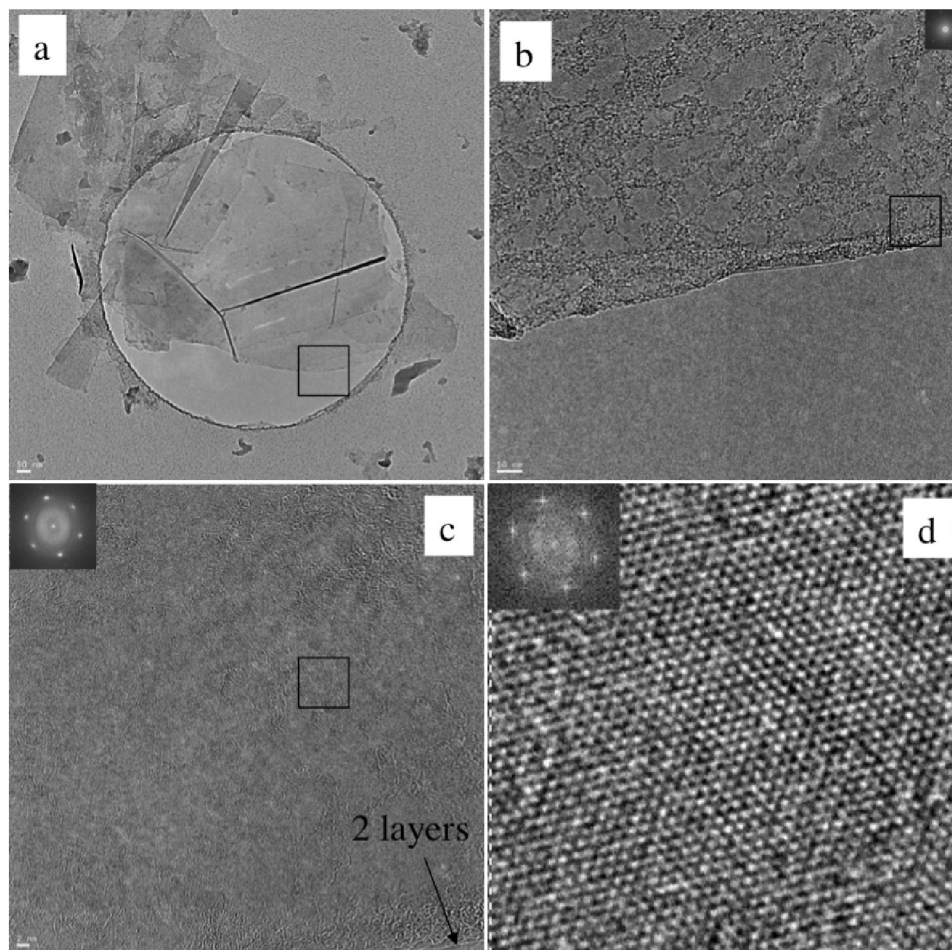
Figure 8.41: TEM images of single layer graphene from HOPG dispersion. (a) monolayer and few layer of graphene stacked with smaller flakes; (b) selected edge region from (a), (c) selected area from (b) with FFT inset, (d) HRTEM of boxed region in (c) showing lattice fringes with FFT inset. Adapted from C. E. Hamilton, PhD Thesis, Rice University (2009).

As-deposited films cast from ODCB graphene show poor electrical conductivity, however, after vacuum annealing at 400 °C for 12 hours the films improve vastly, having sheet resistances on the order of 60 Ω/sq. By comparison, graphene epitaxially grown on Ni has a reported sheet resistance of 280 Ω/sq.

8.4.5 Covalent functionalization of graphene and graphite oxide

The covalent functionalization of SWNTs is well established. Some routes to covalently functionalized SWNTs include esterification/ amidation, reductive alkylation (Billups reaction), and treatment with azomethine ylides (Prato reaction), diazonium salts, or nitrenes. Conversely, the chemical derivatization of graphene and GO is still relatively unexplored.

Some methods previously demonstrated for SWNTs have been adapted to GO or graphene. GO carboxylic acid groups have been converted into acyl chlorides followed by amidation with long-chain amines.

Additionally, the coupling of primary amines and amino acids via nucleophilic attack of GO epoxide groups has been reported. Yet another route coupled isocyanates to carboxylic acid groups of GO. Functionalization of partially reduced GO by aryldiazonium salts has also been demonstrated. The Billups reaction has been performed on the intercalation compound potassium graphite (C_8K), as well as graphite fluoride, and most recently GO. Graphene alkylation has been accomplished by treating graphite fluoride with alkyllithium reagents.

ODCB dispersions of graphene may be readily converted to covalently functionalize graphene. Thermal decomposition of benzoyl peroxide is used to initiate radical addition of alkyl iodides to graphene in ODCB dispersions.

$$\text{(8.17)}$$
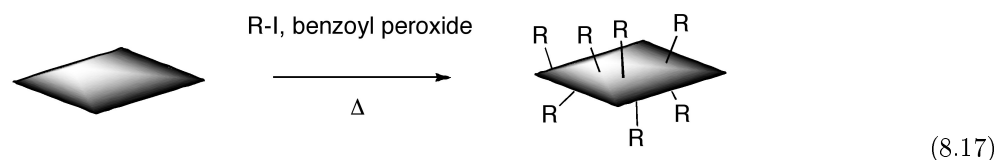
Additionally, functionalized graphene with nitrenes generated by thermal decomposition of aryl azides

$$\text{(8.18)}$$
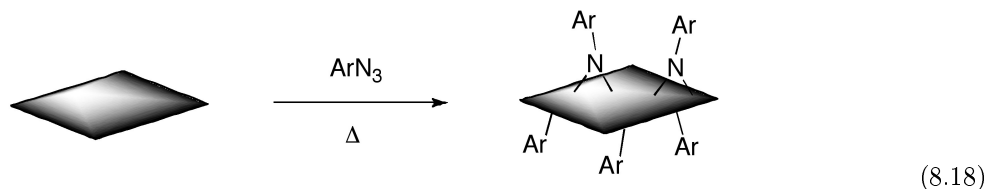
8.4.6 Bibliography

- P. Blake, P. D. Brimicombe, R. R. Nair, T. J. Booth, D. Jiang, F. Schedin, L. A. Ponomarenko, S. V. Morozov, H. F. Gleeson, E. W. Hill, A. K. Geim, and K. S. Novoselov, *Nano Lett.*, 2008, **8**, 1704.
- J. Chattopadhyay, A. Mukherjee, C. E. Hamilton, J.-H. Kang, S. Chakraborty, W. Guo, K. F. Kelly, A. R. Barron, and W. E. Billups, *J. Am. Chem. Soc.*, 2008, **130**, 5414.
- G. Eda, G. Fanchini, and M. Chhowalla, *Nat. Nanotechnol.*, 2008, **3**, 270.
- M. Y. Han, B. Ozyilmaz, Y. Zhang, and P. Kim, *Phys. Rev. Lett.*, 2008, **98**, 206805.
- Y. Hernandez, V. Nicolosi, M. Lotya, F. M. Blighe, Z. Sun, S. De, I. T. McGovern, B. Holland, M. Byrne, Y. K. Gun'Ko, J. J. Boland, P. Niraj, G. Duesberg, S. Krishnamurthy, R. Goodhue, J. Hutchinson, V. Scardaci, A. C. Ferrari, and J. N. Coleman, *Nat. Nanotechnol.*, 2008, **3**, 563.
- W. S. Hummers and R. E. Offeman, *J. Am. Chem. Soc.*, 1958, **80**, 1339.
- L. Jiao, L. Zhang, X. Wang, G. Diankov, and H. Dai, *Nature*, 2009, **458**, 877.
- D. V. Kosynkin, A. L. Higginbotham, A. Sinitskii, J. R. Lomeda, A. Dimiev, B. K. Price, and J. M. Tour, *Nature*, 2009, **458**, 872.
- D. Li, M. B. Mueller, S. Gilje, R. B. Kaner, and G. G. Wallace, *Nat. Nanotechnol.*, 2008, **3**, 101.
- S. Niyogi, E. Bekyarova, M. E. Itkis, J. L. McWilliams, M. A. Hamon, and R. C. Haddon, *J. Am. Chem. Soc.*, 2006, **128**, 7720.
- Y. Si and E. T. Samulski, *Nano Lett.*, 2008, **8**, 1679.
- L. Staudenmaier, *Ber. Dtsch. Chem. Ges.*, 1898, **31**, 1481.

8.5 Rolling Molecules on Surfaces Under STM Imaging[8]

8.5.1 Introduction to surface motions at the molecular level

As single molecule imaging methods such as scanning tunneling microscope (STM), atomic force microscope (AFM), and transmission electron microscope (TEM) developed in the past decades, scientists have gained powerful tools to explore molecular structures and behaviors in previously unknown areas. Among these imaging methods, STM is probably the most suitable one to observe detail at molecular level. STM can operate in a wide range of conditions, provides very high resolution, and able to manipulate molecular motions with the tip. An interesting early example came from IBM in 1990, in which the STM was used to position individual atoms for the first time, spelling out "I-B-M" in Xenon atoms. This work revealed that observation and control of single atoms and molecular motions on surfaces were possible.

The IBM work, and subsequent experiments, relied on the fact that STM tip always exerts a finite force toward an adsorbate atom that contains both van der Waals and electrostatic forces was utilized for manipulation purpose. By adjusting the position and the voltage of the tip, the interactions between the tip and the target molecule were changed. Therefore, applying/releasing force to a single atom and make it move was possible Figure 8.42.
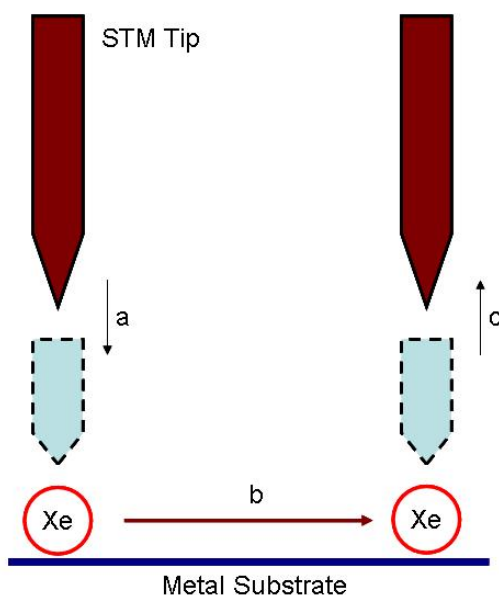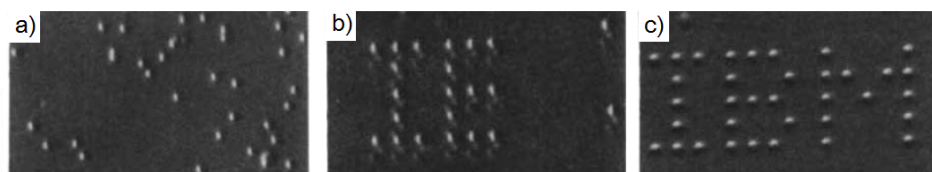

Figure 8.42: Manipulation of STM tip toward a xenon atom. a) STM tip move onto a target atom then change the voltage and current of the tip to apply a stronger interaction. b) Move the atom to a desire position. c) After reaching the desire position, the tip released by switching back to the scanning voltage and current.

The actual positioning experiment was carried out in the following process. The nickel metal substrate was prepared by cycles of argon-ion sputtering, followed by annealing in a partial pressure of oxygen to

---

[8]This content is available online at <http://cnx.org/content/m22965/1.3/>.

remove surface carbon and other impurities. After the cleaning process, the sample was cooled to 4 K, and imaged with the STM to ensure the quality of surface. The nickel sample was then doped with xenon. An image of the doped sample was taken at constant-current scanning conditions. Each xenon atom appears as a located randomly 1.6 Å high bump on the surface (Figure 8.43a). Under the imaging conditions (tip bias = 0.010 V with tunneling current 10^{-9} A) the interaction of the xenon with the tip is too weak to cause the position of the xenon atom to be perturbed. To move an atom, the STM tip was placed on top of the atom performing the procedure depicted in Figure 8.42 to move it to its target. Repeating this process again and again led the researcher to build of the structure they desired Figure 8.43b and c.

Figure 8.43: Manipulation of STM tip starting with a) randomly dosed xenon sample, b) under construction - move xenon atom to desire position, and c) accomplishment of the manipulation. Adapted from D. M. Eigler and E. K. Schweizer, *Nature*, 1990, **344**, 524.

All motions on surfaces at the single molecule level can be described as by the following (or combination of the following) modes:

  i. Sliding.
 ii. Hopping.
iii. Rolling.
 iv. Pivoting.

Although the power of STM imaging has been demonstrated, imaging of molecules themselves is still often a difficult task. The successful imaging of the IBM work was attributed to selection of a heavy atom. Other synthetic organic molecules without heavy atoms are much more difficult to be imaged under STM. Determinations of the mechanism of molecular motion is another. Besides imaging methods themselves, other auxiliary methods such as DFT calculations and imaging of properly designed molecules are required to determine the mechanism by which a particular molecule moves across a surface.

Herein, we are particularly interested in surface-rolling molecules, i.e., those that are designed to roll on a surface. It is straightforward to imagine that if we want to construct (and image) surface-rolling molecules, we must think of making highly symmetrical structures. In addition, the magnitudes of interactions between the molecules and the surfaces have to be adequate; otherwise the molecules will be more susceptible to slide/hop or stick on the surfaces, instead of rolling. As a result, only very few molecules are known can roll and be detected on surfaces.

8.5.2 Surface rolling of molecules under the manipulation of STM tips

As described above, rolling motions are most likely to be observed on molecules having high degree of symmetry and suitable interactions between themselves and the surface. C_{60} is not only a highly symmetrical molecule but also readily imageable under STM due to its size. These properties together make C_{60} and its derivatives highly suitable to study with regards to surface-rolling motion.

The STM imaging of C_{60} was first carried out at At King College, London. Similar to the atom positioning experiment by IBM, STM tip manipulation was also utilized to achieve C_{60} displacement. The tip trajectory

suggested that a rolling motion took into account the displacement on the surface of C_{60}. In order to confirm the hypothesis, the researchers also employed *ab initio* density function (DFT) calculations with rolling model boundary condition (Figure 8.44). The calculation result has supported their experimental result.
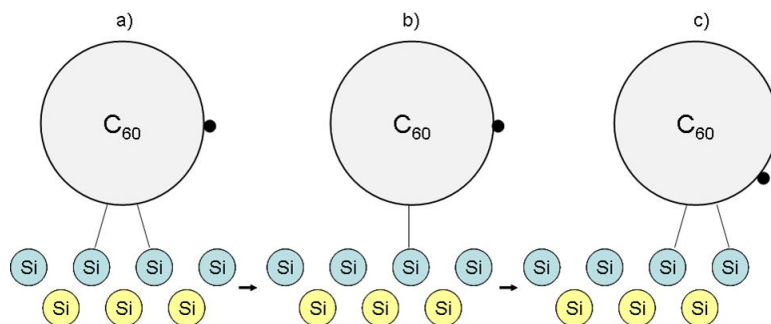
Figure 8.44: Proposed mechanism of C_{60} translation showing the alteration of C_{60}··surface interactions during rolling. a) 2-point interaction. The left point interaction was dissociated during the interaction. b) 1-point interaction. C_{60} can pivot on surface. c) 2-point interaction. A new interaction formed to complete part of the rolling motion. a) - c) The black spot on the C_{60} is moved during the manipulation. The light blue Si balls represent the first layer of molecules the silicon surface, and the yellow balls are the second layer.

The results provided insights into the dynamical response of covalently bound molecules to manipulation. The sequential breaking and reforming of highly directional covalent bonds resulted in a dynamical molecular response in which bond breaking, rotation, and translation are intimately coupled in a rolling motion (Figure 8.45), but not performing sliding or hopping motion.

A triptycene wheeled dimeric molecule Figure 8.45 was also synthesized for studying rolling motion under STM. This "tripod-like" triptycene wheel ulike a ball like C_{60} molecule also demonstrated a rolling motion on the surface. The two triptycene units were connected via a dialkynyl axle, for both desired molecule orientation sitting on surface and directional preference of the rolling motion. STM controlling and imaging was demonstrated, including the mechanism Figure 8.45.
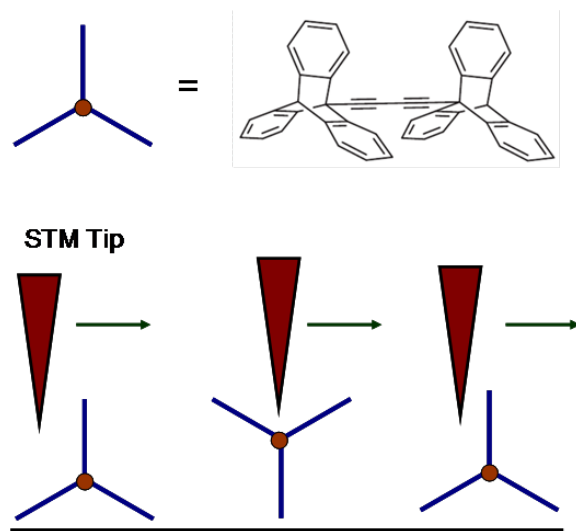
Figure 8.45: Scheme of the rolling mechanism (left to right). Step 1 is the tip approach towards the molecule, step 2 is a 120 degree rotation of a wheel around its molecular axle and in step 3 the tip reaches the other side of the molecule. It shows that, in principle, only one rotation of a wheel can be induced (the direction of movement is marked by arrows).

### 8.5.3 Single molecule nanocar under STM imaging

Another use of STM imaging at single molecule imaging is the single molecule nanocar by the Tour group at Rice University. The concept of a nanocar initially employed the free rotation of a C-C single bond between a spherical C_{60} molecule and an alkyne, Figure 8.46. Based on this concept, an "axle" can be designed into which are mounted C_{60} "wheels" connected with a "chassis" to construct the "nanocar". Nanocars with this design are expected to have a directional movement perpendicular to the axle. Unfortunately, the first generation nanocar (named "nanotruck" Figure 8.47) encountered some difficulties in STM imaging due to its chemical instability and insolubility. Therefore, a new of design of nanocar based on OPE has been synthesized Figure 8.48.
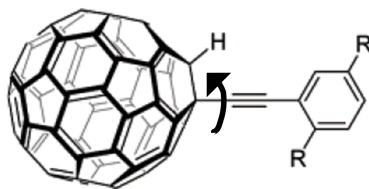
Figure 8.46: Structure of C_{60} wheels connecting to an alkyne. The only possible rolling direction is perpendicular to the C-C single bond between C_{60} and the alkyne. The arrow indicates the rotational motion of C_{60}.
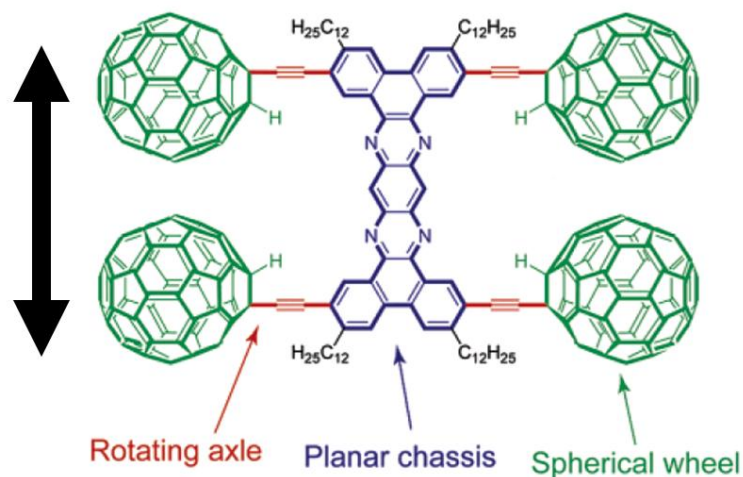

Figure 8.47: Structure of the nanotruck. No rolling motion was observed under STM imaging due to its instability, insolubility and inseparable unreacted C_{60}. The double head arrow indicates the expected direction of nanocar movement. Y. Shirai, A. J. Osgood, Y. Zhao, Y. Yao, L. Saudan, H. Yang, Y.-H. Chiu, L. B. Alemany, T. Sasaki, J.-F. Morin, J. M. Guerrero, K. F. Kelly, and J. M. Tour, *J. Am. Chem. Soc.*, 2006, **128**, 4854. Copyright American Chemical Society (2006).
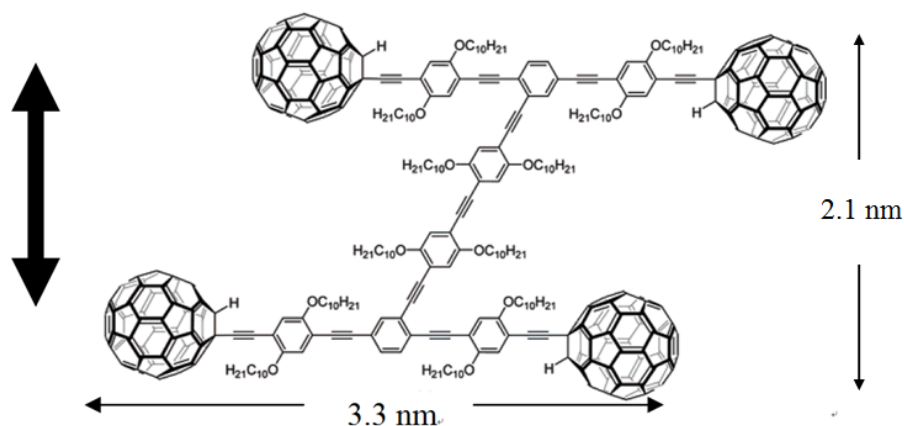
Figure 8.48: Nanocar based on OPE structure. The size of the nanocar is 3.3 nm X 2.1 nm (W x L). Alkoxy chains were attached to improve solubility and stability. OPE moiety is also separable from C_{60}. The bold double head arrow indicates the expected direction of nanocar movement. The dimension of nanocar was 3.3 nm X 2.1 nm which enable direct observation of the orientation under STM imaging. Y. Shirai, A. J. Osgood, Y. Zhao, K. F. Kelly, and J. M. Tour, *Nano Lett.*, 2005, **5**, 2330. Copyright American Chemical Society (2005).

The newly designed nanocar was studied with STM. When the nanocar was heated to ~200 °C, noticeable displacements of the nanocar were observed under selected images from a 10 min STM experiment Figure 8.49. The phenomenon that the nanocar moved only at high temperature was attributed their stability to a relatively strong adhesion force between the fullerene wheels and the underlying gold. The series of images showed both pivotal and translational motions on the surfaces.
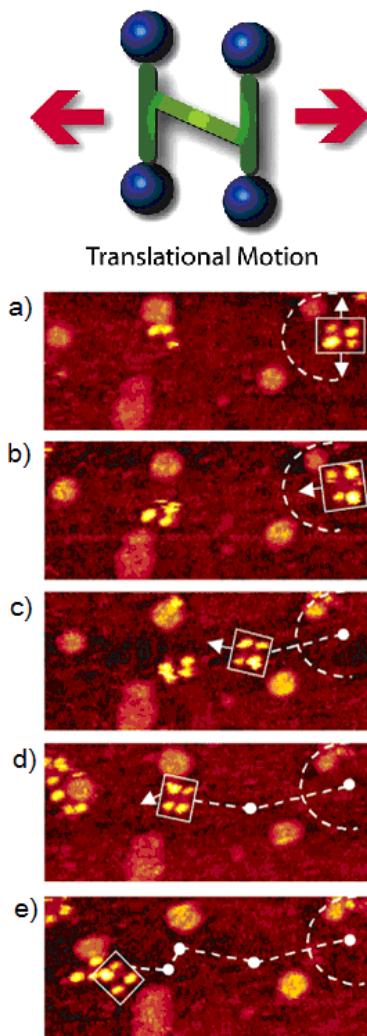
Figure 8.49: Pivotal and translational movement of OPE based nanocar. Acquisition time of one image is approximately 1 min with (a – e) images were selected from a series spanning 10 min. The configuration of the nanocar on surface can be determined by the distances of four wheels. a) – b) indicated the nanocar had made a 80° pivotal motion. b) – e) indicated translation interrupted by small-angle pivot perturbations. Y. Shirai, A. J. Osgood, Y. Zhao, K. F. Kelly, and J. M. Tour, *Nano Lett.*, 2005, **5**, 2330. Copyright American Chemical Society (2005).

Although literature studies suggested that the C_{60} molecule rolls on the surface, in the nanocar movement studies it is still not possible to conclusively conclude that the nanocar moves on surface exclusively via a rolling mechanism. Hopping, sliding and other moving modes could also be responsible for the movement of the nanocar since the experiment was carried out at high temperature conditions, making the C_{60} molecules more energetic to overcome interactions between surfaces.

To tackle the question of the mode of translation, a trimeric "nano-tricycle" has been synthesized. If the movement of fullerene-wheeled nanocar was based on a hopping or sliding mechanism, the trimer should give

observable translational motions like the four-wheeled nanocar, however, if rolling is the operable motion then the nano-tricycle should rotate on an axis, but not translate across the surface. The result of the imaging experiment of the trimer at $\sim$200 °C (Figure 8.50,) yielded very small and insignificant translational displacements in comparison to 4-wheel nanocar (Figure 8.49). The trimeric 3-wheel nanocar showed some pivoting motions in the images. This motion type can be attributed to the directional preferences of the wheels mounted on the trimer causing the car to rotate. All the experimental results suggested that a C_{60}-based nanocar moves via a rolling motion rather than hopping and sliding. In addition, the fact that the thermally driven nanocar only moves in high temperature also suggests that four C_{60} have very strong interactions to the surface.
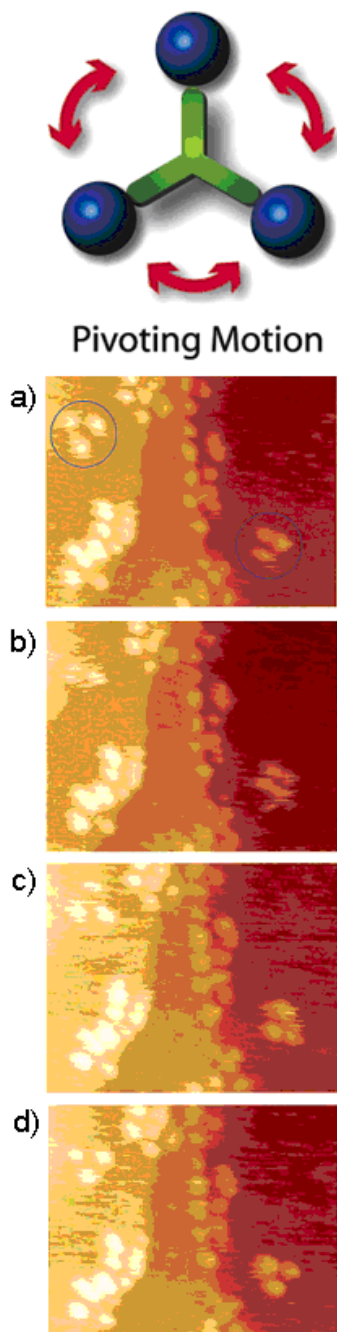
Figure 8.50: Pivot motion of the trimer. a) - d) Pivot motions of circled trimered were shown in the series of images. No significant translation were observed in comparison to the nanocar. Y. Shirai, A. J. Osgood, Y. Zhao, K. F. Kelly, and J. M. Tour, *Nano Lett.*, 2005, **5**, 2330. Copyright American Chemical Society (2005).

8.5.4 Bibliography

- D. M. Eigler and E. K. Schweizer, *Nature*, 1990, **344**, 524.
- L. Grill, K. -H. Rieder, F. Moresco, G. Rapenne, S. Stojkovic, X. Bouju, and C. Joachim, *Nat. Nanotechnol.*, 2007, **2**, 95.
- Y. Shirai, A. J. Osgood, Y. Zhao, K. F. Kelly, and J. M. Tour, *Nano Lett.*, 2005, **5**, 2330.
- Y. Shirai, A. J. Osgood, Y. Zhao, Y. Yao, L. Saudan, H. Yang, Y.-H. Chiu, L. B. Alemany, T. Sasaki, J.-F. Morin, J. M. Guerrero, K. F. Kelly, and J. M. Tour, *J. Am. Chem. Soc.*, 2006, **128**, 4854.